



Published in final edited form as:

*Expert Opin Drug Discov.* 2017 July ; 12(7): 711–731. doi:10.1080/17460441.2017.1331216.

## Rational Design Strategies for FimH Antagonists: New Drugs on the Horizon for Urinary Tract Infection and Crohn's Disease

Laurel K. Mydock-McGrane<sup>a</sup>, Thomas J. Hannan<sup>a</sup>, and James W. Janetka<sup>b,\*</sup>

<sup>a</sup>Fimbrion Therapeutics, Inc., Washington University School of Medicine, Saint Louis, MO 63108 USA

<sup>b</sup>Department of Biochemistry and Molecular Biophysics, Washington University School of Medicine, Saint Louis, MO 63108 USA

### Abstract

**Introduction**—The bacterial adhesin FimH is a virulence factor and an attractive therapeutic target for urinary tract infection (UTI) and Crohn's Disease (CD). Located on type 1 pili of uropathogenic *E. coli* (UPEC), the FimH adhesin plays an integral role in the pathogenesis of UPEC. Recent efforts have culminated in the development of small-molecule mannoside FimH antagonists that target the mannose-binding lectin domain of FimH, inhibiting its function and preventing UPEC from binding mannosylated host cells in the bladder, thereby circumventing infection.

**Areas covered**—The authors describe the structure-guided design of mannoside ligands, and review the structural biology of the FimH lectin domain. Additionally, they discuss the lead optimization of mannosides for therapeutic application in UTI and CD, and describe various assays used to measure mannoside potency *in vitro* and mouse models used to determine efficacy *in vivo*.

**Expert opinion**—To date, mannoside optimization has led to a diverse set of small-molecule FimH antagonists with oral bioavailability. With clinical trials already initiated in CD and on the horizon for UTI, it is the authors opinion that mannosides will be a 'first-in-class' treatment strategy for UTI and CD, and will pave the way for treatment of other Gram-negative bacterial infections.

### 1. Introduction

Urinary tract infections (UTIs) are one of the most common infectious diseases worldwide, with greater than 85% of these infections caused by the Gram-negative bacteria, uropathogenic *Escherichia coli* (UPEC) [1]. Especially prevalent in women, it is estimated that more than half of all women will experience a UTI in their lifetime [2-4]. Standard of care therapy for uncomplicated UTI is a short course of antibiotics, which is typically highly

---

Contact: janetkaj@biochem.wustl.edu.

**Declaration of Interest:** JW Janetka is a co-founder and stockholder of Fimbrion Therapeutics, Inc., and TJ Hannan and LK Mydock-McGrane are employees of Fimbrion who also hold company stock options. The authors have no other relevant affiliations or financial involvement with any organization or entity with a financial interest in or financial conflict with the subject matter or materials discussed in the manuscript apart from those disclosed.

effective against sensitive UPEC strains. However, despite appropriate use of antibiotics, UTIs recur at a very high rate with 25-35% of patients having a second infection within 6 months of an acute episode. Thus, UTIs account for 5% of all antibiotic prescriptions, and antibiotic resistant strains of UPEC are becoming increasingly common in the urine cultures of infected persons [5-9]. With the latency in development of new-antibiotics, there is a dire need for new therapeutic approaches [10-11] to eliminating bacterial infections.

One such therapeutic approach, is to target the virulence factors [12-14] involved in the bacterial adhesion of UPEC to the urothelial surface. Rather than aiming to kill the bacteria, as is the focus of common UTI antibiotics, such as trimethoprim-sulfamethoxazole and fluoroquinolones, this novel anti-adhesive approach [11, 15] serves only to 'disarm' the bacteria, thereby avoiding the strong selective pressure of viability that leads to bacterial resistance. Antibiotic resistance is exponentially increasing for all Gram-negative infections, but especially in UTI [6-7], highlighted recently by the first case in the United States of a UTI patient carrying pandrug resistant (PDR) *E. coli* bearing the *mcr-1* gene and that did not respond to the last line antibiotic colistin [16-17].

### 1.1 Structure and function of type 1 pili and FimH

In the case of UPEC, adhesion is facilitated through the binding of the FimH lectin to mannosylated glycoproteins that coat the bladder epithelium [18-20] (Fig. 1). This mannose-specific FimH lectin is located at the distal tip of type 1 pili, a class of pili which are highly expressed on the bacterial surface of UPEC and other Gram-negative uropathogens. Projecting outward from the bacterial surface, these long hair-like appendages are comprised of a long pilus rod of repeating FimA pilin subunits, and a tip fibrillum, which consists of one FimF and FimG pilin subunit each, and is capped by a single FimH adhesin. The FimH adhesin itself is made up of two domains, the C-terminal pilin domain (FimH<sub>PD</sub>) that anchors the adhesin to the pilus rod, and the N-terminal lectin domain (FimH<sub>LD</sub>) which houses the mannose-binding pocket.

A natural receptor of the FimH lectin, is the highly mannosylated uroplakin Ia (UPIa) glycoprotein, which is a glycosylation-dependent receptor present on the surface of epithelial umbrella cells of the urinary tract [21]. This abundantly expressed glycoprotein is decorated by a specific sequence of branched oligomannose structures, which the FimH adhesin recognizes and binds. It is this attachment that initiates the UPEC infection cycle, enabling bacterial invasion, colonization, proliferation and the subsequent formation of biofilm-like intracellular bacterial communities (IBCs) within bladder epithelial cells. Experimental murine models of UTI have recapitulated clinically relevant human UTI scenarios, such as acute, chronic, recurrent and catheter-associated bladder infections. The presence of FimH is essential to both UPEC pathogenicity in these animal models, as well as bacterial biofilm formation, highlighting FimH as a key virulence factor in UTI pathogenesis. This makes the inhibition of FimH function an effective way to disarm and disable the UPEC bacteria, and as such, there has been a growing interest in the development of FimH antagonists as a novel, antibiotic-sparing therapeutic approach to combat UTIs.

Though much work on the development of FimH antagonists is focused on UTIs, it should also be acknowledged that more recently, the FimH adhesin displayed on the type 1 pili of

another bacterial pathotype, known as adherent and invasive *E. coli* (AIEC), has also been found to play a significant role in the pathogenicity of Crohn's disease (CD) disease. In these cases, chronic inflammation of the ileal epithelium leads to over-expression of the highly-mannosylated, carcinoembryonic antigen-related cell adhesin molecule 6 (CEACAM6), which FimH can then bind to, enabling AIEC to adhere to and invade the gut mucosa. Current results have been promising, clearly demonstrating the ability of FimH antagonists to both decrease the AIEC population and mitigate the inflammatory response [22].

## 1.2 Initial Discovery of FimH ligands based on $\alpha$ -D-mannose

The first mention of mannose as a possible inhibitor of *E. coli* attachment to intestinal epithelial cells was reported back in 1957 [23], but remained unnoticed until the seminal work by Nathan Sharon in 1977 [24]. In this paper, they presented the first solid data on the mannose-mediated attachment of *E. coli* K<sub>12</sub> and B strains to human epithelial cells, and reported the presence of a "lectin-like" substance on the surface of *E. coli*, which would eventually become known as FimH. Through competitive inhibition experiments, it was found that both  $\alpha$ -D-mannose and methyl  $\alpha$ -D-mannopyranoside ( $\alpha$ MM) (Fig. 2) could both prevent *E. coli* from binding to epithelial cells, and displace pre-attached *E. coli* from epithelial cells. In 1979, the first mouse study was reported [25], wherein  $\alpha$ MM was used as a prophylactic to prevent the colonization of *E. coli* within the urinary tract. From this proof-of-concept study, the FimH lectin emerged as a promising therapeutic target to combat UTIs. Throughout the 1980s, several groups [26-30] began efforts aimed at designing more effective FimH inhibitors. During this period, a variety of synthetic mannosides and naturally occurring oligosaccharides isolates, were further identified as inhibitors of the FimH lectin. This pioneering research laid the foundation in which the future generations of rationally designed, potent and orally bioavailable, small-molecule FimH mannoside antagonists [31] would be built upon.

Herein, we comprehensively review rational ligand design and drug discovery strategies which have been employed to generate high-affinity, monovalent inhibitors of FimH. We first describe structural aspects of the FimH binding pocket and how modifications affect ligand binding affinity and potency. Next, we discuss the medicinal chemistry approaches toward lead optimization as drugs, for the oral treatment of urinary tract infections (UTIs) and other FimH-dependent disease such as Crohn's Disease (CD).

## 2. Overview of the *in vitro* binding and functional assays of FimH activity

Over the last 20 years, multiple *in vitro* assays have been utilized to measure both the binding affinity to, and functional potency against FimH. The lack of a universal assay used by all for determining FimH activity, has also led to some difficulty when trying to compare relative potencies reported in the various assays. To help bring some clarity to this ongoing issue, we describe the different binding assays and functional assays, and their use in screening FimH activity, and provide some examples which have data across multiple assays (Table 1).

## 2.1. FimH competitive binding assays

**2.1.1. Cell-free FimH binding assay**—A high-throughput binding assay has been developed by the Ernst group to compare potency of FimH antagonists [32-33]. The assay utilizes recombinant truncated FimH protein, containing only the carbohydrate recognition domain (CRD). FimH is immobilized and FimH antagonists compete for binding against a biotinylated polyacrylamide glycopolymer.

**2.1.2. ELISA (enzyme-linked immunosorbent assay) type assays**—To determine the potencies of mannosides as inhibitors of type 1 fimbriae-mediated adhesion of *E. coli*, an ELISA was developed [34]. Results are reported as RIP (relative inhibitory potency) vs.  $\alpha$ MM, which has a defined  $IC_{50}$  of 1. A variation of an ELISA called the ELLSA (enzyme-linked lectinosorbent assay) uses immobilized RNaseB, a mannosylated glycoprotein [35-36], that is incubated with recombinant FimH, with or without FimH antagonists, and the binding of FimH to RNaseB detected by anti-FimH antibodies.

**2.1.3. Fluorescence polarization (FP) binding**—This assay relies on the use of a fluorescently labeled mannoside FimH ligand. In this case, a Fluorescein-labeled butyl mannoside derivative was utilized to determine the  $IC_{50}$  values of synthetic mannosides when in competition with the labeled ligand[37-38].

**2.1.4. Radiolabel binding**—A standard competitive binding assay which uses radiolabeled D-mannose as the FimH ligand to compete with other mannoside ligands, was utilized to determine the thermodynamic binding parameters ( $\Delta G$ ,  $S$ ,  $H$ ), and calculate the quantitative binding affinity ( $K_D$ ) of early mannosides [39].

**2.1.5. Isothermal titration calorimetry (ITC)**—In one recent paper, the Ernst group has employed the use of ITC for determining the kinetics and thermodynamics of FimH ligand binding [40]. This assay is low throughput but provides the most accurate and precise measurements of FimH ligand binding interactions, allowing for the best determination of  $K_D$ , equilibrium binding affinities.

**2.1.6. Surface Plasmon Resonance (SPR) and Biolayer Interferometry (BLI)**—Modern assays used to determine mannoside binding kinetics include SPR [39] and BLI [41]. In SPR, FimH is immobilized on a sensory chip and changes in plasmon resonance are used to detect association/binding with FimH by mannosides in solution. BLI is similar, but uses a fiber optic biosensor with a coating at the tip. In this method, biotinylated FimH is immobilized on the tip and then mannoside binding is detected by a shift in the wavelength of the applied light. BLI is higher throughput and less prone to issues caused by experimental conditions than SPR, but is less sensitive.

**2.1.7. Differential Scanning Fluorimetry (DSF)**—BLI can not be used to calculate a binding affinity for high affinity mannoside, due to slow off-rates. Therefore, a DSF (or ‘melting point’) assay was developed to circumvent this problem [41]. This assay measures the change in temperature ( $\Delta T$ ) of the denaturation point of FimH upon mannoside binding, relative to that of FimH alone, where  $\Delta T$  is proportional to the free energy of binding

[42-43]. T for individual mannosides correlates well with the activity in the HAI and biofilm cell assays, providing an efficient method for ranking ligand binding affinities.

## 2.2. Functional inhibition assays of FimH activity

**2.2.1. Aggregation Assay**—The earliest technique to evaluate the functional activity of FimH antagonists was a cell-based bacterial aggregation assay, built on the ability of FimH-expressing *E. coli* to cause the aggregation of mannan-containing yeast cells [26, 29]. By measuring the increasing light transmitted upon aggregation, FimH-antagonists were ranked on decreases in the rate of aggregation, at varying concentrations of mannoside.

**2.2.2. Hemagglutination Inhibition (HAI) Assay**—A more accurate assay, called the hemagglutination assay (HA), was first developed by Hultgren in 1986 [44], and has since been used a standard measure of FimH antagonist potency in subsequent publications [37, 41, 45-46]. This assay is a variation of the aggregation assay, with better accuracy and suited for high-throughput screening. It is based on the ability of *E. coli* to aggregate (or agglutinate) guinea pig erythrocytes (GPEs), *via* FimH-mediated adherence of *E. coli* to the glycocalyx of GPEs. FimH antagonists are pre-incubated with *E. coli* and are then assigned an HAI titer, which relates to the minimum concentration of antagonist necessary to inhibit >90% of the agglutination (HAI or EC<sub>90</sub>). For context, the HAI titer of  $\alpha$ MM is >1 mM and heptyl mannoside (HM) is 15  $\mu$ M. Recent mannosides generally have an HAI titer in the range of 100 nM to 1  $\mu$ M, with optimized compounds now below 10 nM [45].

**2.2.3. Disaggregation Assay**—Abgottspon *et al.* [47] remodeled the HAI assay into a so-called ‘disaggregation’ assay. Aggregation is first achieved by the incubation of *E. coli* with either *Candida albicans* yeast, or with GPEs. The FimH antagonist is then added, and disaggregation is determined by light transmission over time, and reported using IC<sub>50</sub> values. For reference,  $\alpha$ MM showed no quantifiable disaggregation, whereas HM has an IC<sub>50</sub> = 77  $\mu$ M.

**2.2.4. Biofilm inhibition**—One assay was developed [48-50] to quantitatively measure a compound's ability to disrupt assembly of a bacterial biofilm. Biofilms are capable of evading and enduring standard antibiotic therapies for UTIs, greatly adding to recurrence and resistance mechanisms [51]. Briefly, bacteria are grown in the presence of FimH antagonist at varied concentrations and the biofilm is stained. This assay is utilized frequently [41, 46], with the most potent mannosides displaying IC<sub>50</sub> values less than 20 nM [46].

**2.2.5. Inhibition of epithelial cell adherence**—A different type of assay quantitates the effect of FimH antagonists directly to a human bladder epithelial cell line [52], and AIEC binding to a human colonic cell line [35]. The assay can be performed under flow or non-flow conditions, with the former employed to mimic bacterial binding in the bladder where urine is under intermittent flow. This has relevance to the development of drugs to treat UTI, since the FimH lectin domain exists dynamically in several distinct forms [53-55], having different affinities for mannoside ligands.

### 3. Murine animal models of UTI and Crohn's Disease (CD)

#### 3.1. Mouse models of urinary tract infection (UTI)

Current standard of care treatment of human cystitis typically requires a 3 to 5-day course of antimicrobials for treatment of an active infection, or daily antimicrobial dosing for prophylaxis. Therefore, in developing lead FimH antagonists, it is imperative not only to demonstrate proof of concept activity in a relevant animal model, but also to demonstrate efficacy in animal models that resemble the specific clinical indication. The Hultgren laboratory and others have developed mouse models of acute, recurrent, and chronic cystitis that reflect aspects of first time UTI, recurrent UTI (rUTI), and chronic UTI, respectively, in humans [56-58]. Using these models, different classes of FimH antagonist compounds have been shown to be orally bioavailable and have potent, fast-acting efficacy in mouse models of UTI at doses as low as 10 mg/kg and maintaining efficacy for up to 12 hours [38, 45].

**3.1.1. Prophylactic (Prevention of infection) Models**—UPEC have been shown to not only colonize, but also to invade and massively replicate inside the superficial facet cells of mouse urothelium, rapidly forming intracellular bacterial communities (IBCs) that bypass the innate resistance of the urinary bladder to colonization [20, 59]. In fact, IBC formation has been demonstrated to be a population bottleneck in UPEC pathogenesis in the mouse model, such that preventing IBC formation can result in an aborted infection [60-61]. Therefore, mice treated orally with potent FimH antagonists shortly before experimental infection with UPEC show a dramatic reduction in IBCs at 6 hours post-infection (hpi), translating to a several log reduction in bladder bacterial burden [62].

The efficacy of FimH antagonists in this C3H/HeN acute prophylactic model has been demonstrated against several UPEC strains, including two multidrug resistant UPEC strains [62-63]. A variation of the prophylactic model, is the use of diuresis, through providing 5% glucose in the drinking water 3 days prior to infection, which for unknown reasons exacerbates acute UTI [32, 64]. The Ernst group has used this variation to accentuate the protective effect of their FimH antagonists when given prior to infection, with tissues examined at 3 hpi [32, 38]. Furthermore, C3H mice are genetically susceptible to vesicoureteral reflux (VUR), meaning that inoculation of bacteria into the bladder almost always leads to reflux of bacteria up the ureters and kidneys [65]. FimH antagonists do not affect this reflux (VUR), which is not dependent upon FimH function. Other mouse strains, such as C57BL/6J, are resistant to VUR and should be investigated for use in this model. Further development of this model is needed to move beyond proof of concept and translate it to more clinically relevant situations. This would include expanding the number of UPEC strains tested against lead FimH antagonists, extending the time between dosing and infection with dosages that approximate a reasonable human dose, and translating the prophylactic model to the rUTI mouse model.

The ability to prevent UPEC invasion into the bladder tissue and restrict the bacteria to the lumen, can potentially enable first-line antimicrobials to be effective against UPEC strains that have acquired antibiotic resistance. This was demonstrated by in experiments where mice were infected with a UPEC strain that was clinically resistant to trimethoprim-sulfamethoxazole (TMP-SMZ) and treatment with TMP-SMZ during acute infection had no



effect on bladder bacterial burdens [62]. However, if the mice were treated prior to infection with a FimH antagonist, TMP-SMZ treatment caused a further reduction in bladder bacterial beyond antagonist alone. Measurement of antimicrobial concentrations in the urine following TMP-SMZ treatment revealed that TMP levels reached 9 mg/ml in the urine, well above the 256 µg/ml minimum inhibitory concentration (MIC) of the resistant strain. These results suggest that by preventing invasion of bladder epithelial cells, FimH antagonists compartmentalize UPEC bacteria to the bladder lumen, thereby exposing them to TMP-SMZ concentrations well above the MIC of even a clinically resistant strain, resulting in bacterial cell death. It is likely that during standard treatment, TMP-SMZ reaches tissue levels above the MIC needed for killing of sensitive strains but fails to reach tissue levels needed for killing PBC-1.

Translated to clinical practice, FimH antagonists could be a cost-effective “antimicrobial-sparing” treatment that prevents rUTI occurrences without the need for long-term suppressive antibacterial therapy. Furthermore, even if breakthrough rUTI does occur, FimH antagonists restrict UPEC to the bladder lumen and therefore may restore clinical bacterial susceptibility to first-line antimicrobials that concentrate in the urine against multidrug-resistant UPEC in cases, preserving the use of second- and third-line antimicrobials, such as fluoroquinolones and carbapenems, for life-threatening infections.

**3.1.2. Therapeutic (treatment of infection) models**—Another possible clinical indication for FimH antagonists is their use to treat an existing UTI, either alone or as an adjunct therapy to traditional first-line antimicrobials. A simple model for proof of concept of this indication is the treatment of C3H/HeN mice with a chronic bladder infection (chronic cystitis) [56, 62]. While standard of care antimicrobial therapy is highly effective against susceptible UPEC strains, chronic UTI occurs clinically and is an increasing concern with the rise of multidrug resistant UPEC strains [66].

In the chronic cystitis model, C3H/HeN mice are infected with UPEC and the urines of mice are monitored over the following two weeks. Previously, it was demonstrated that the presence of persistent high titer ( $>10^4$  CFU/mL) bacteriuria over this time is a sensitive and specific indicator of chronic cystitis, which is additionally defined by the presence high titer ( $>10^4$  CFU) bladder colonization and chronic bladder inflammation. Most mice will develop chronic cystitis when given a high dose ( $10^8$  or more) of virulent UPEC and 14 days after infection these mice can be then treated with FimH antagonists, either once or several times, and urinary tissues analyzed for bacterial burdens. The benefit of this treatment model is that UPEC are predominantly extracellular during chronic cystitis, so the clear majority of bacteria are exposed to antagonist concentrations in the urine. However, a drawback is that most mice also have kidney infections, that can be variable with some scarring and abscess formation in a subset of mice [56]. A single treatment of chronic cystitis with a potent, bioavailable FimH antagonist led to 1000-fold or more reductions in bladder bacterial burdens 6 hours after treatment of infections with either antimicrobial susceptible or multidrug resistant UPEC strains [62-63]. However, kidney bacterial burdens are not affected and some bladder infections rebounded 24 hours after a single infection, possibly seeded from the kidneys. Three treatments every 8 hours suppresses this rebound effect, but

a bacteriological “cure” may be difficult to achieve in this model because of the persistent kidney reservoir.

### 3.2. Crohn's Disease (CD)

Beyond UTI, FimH antagonists have application to other clinical indications, most notably in the treatment of Crohn's Disease (CD). FimH expressing AIEC are commonly found bound to the ileal mucosa of patients suffering from CD and there is significant phylogenetic overlap between the AIEC and UPEC pathotypes, suggesting that properties that enhance virulence in the urinary tract may also enhance pathogenicity in CD patients. In fact, AIEC recognize and invade intestinal epithelial cells in a type 1 pilus-dependent manner, similar to UPEC adherence and invasion of bladder epithelial cells [67]. The receptor for FimH has been demonstrated to be CEACAM6 that is expressed by chronically inflamed gut epithelium and an animal model for investigating the role of AIEC in Crohn's disease pathogenesis has been developed [68].

In this model, transgenic CEABAC10 mice containing a bacterial artificial chromosome expressing several human CEACAMs, including CEACAM6, are colonized by AIEC in a FimH-dependent manner and Crohn's-like clinical signs and pathology within days of inoculation. To overcome gut colonization resistance, the mice are treated with dextran sulfate sodium (DSS) in the drinking water for three days prior to infection as well as with streptomycin 24 hours prior to infection to disrupt the gut microbiota and cause intestinal inflammation. A high inoculum of  $>10^9$  CFU of the AIEC strain LF82 is given orally and mice are monitored for weight loss and fecal AIEC titers, and ileal tissues analyzed for bacterial burdens, AIEC colonization, and histopathology [68]. To test the efficacy of oral FimH antagonists in preventing Crohn's-like clinical signs and pathology in this mouse CEABAC10 model, mice were treated with 10 mg/kg of candidate compounds at 2 and 18 hpi and monitored over 3-4 days for weight loss, fecal and/or tissue titers, and ileal tissue histopathology and soluble mediators of inflammation [22, 69]. The FimH antagonists tested in these publications all showed efficacy in preventing Crohn's-like clinical signs and pathology, demonstrating the proof of concept that FimH antagonists could potentially be used to treat Crohn's symptoms in patients. A variation of this model utilized ileal loops from CEABAC10 mice that were infected *ex vivo* with LF82, with or without FimH antagonists. In this model [35], demonstrated that a compound could inhibit AIEC colonization of the ileum.

## 4. Structural biology of type 1 pili, FimH and its lectin D-mannose binding pocket

As mentioned above, type 1 pili are comprised of repeating FimA pilin subunits, and a tip fibrillum, which consists of one FimF and FimG pilin, capped by the FimH adhesin (Fig. 1B). Type 1 and other Pili fibers are constructed by the Chaperone Usher Pathway (CUP), in which coordinated orchestration of strand donation events drive pilus assembly [70-74]. The adhesin FimH consists of two domains, the C-terminal pilin domain (FimH<sub>PD</sub>) that anchors it to the pilus rod, and the N-terminal lectin domain (FimH<sub>LD</sub>) which houses the mannose-binding pocket. In 2002, the first X-ray crystal structure of  $\alpha$ -D-mannose bound to the



FimCH chaperone-adhesin complex was obtained [75] and shortly thereafter in 2005, a serendipitous discovery was made by Bouckaert et. al. [39], of a butyl  $\alpha$ -D-mannopyranoside bound within the crystal structures of the truncated FimH lectin domains of both UPEC96 and G1655 (an *E. coli* K-12 laboratory strain). Subsequently [76], the structure of the branched pentasaccharide, oligomannose-3 (Fig. 3A), was reported. These initial studies profiled the mannose binding site of FimH, and defined the molecular-level interactions of FimH with both D-mannose and its mannosylated receptor ligand.

The FimH lectin domain is comprised of amino acid residues 1-157, which form an elongated 11-stranded  $\beta$ -barrel structure. The domain is comprised of a polar mannose-binding pocket (Fig. 3, red: Asn46, Asp47, Asp54, Gln133, Asn135, Asn138 and Asp140) in which the sugar participates in multiple hydrogen bonding and electrostatic interactions with FimH. Surrounding this tight pocket is a hydrophobic region, which is comprised of the hydrophobic support (Fig. 3, grey: Phe1, Ile13, and Phe142), the 'tyrosine gate' (Fig. 3, blue: Tyr48, Ile52 and Tyr137) and residue Thr51 (Fig. 3, cyan) [76]. Other distinguishing features of the lectin domain include: 1) a small hydrophobic pocket that exists adjacent to the sugar-binding pocket, defined by residues Ile52, Tyr137 and Asn138 [46]; 2) the Arg98-Glu50 salt bridge [37]; and 3) the Tyr48 and Tyr137 hydroxyl groups which can form H-bonding interactions with the aglycones of mannoside ligands [37, 46]; Mannosides have been rationally designed to make interactions with these residues, resulting in significant augmentation of FimH binding affinity.

#### 4.1. FimH sugar-binding pocket: Selectivity for $\alpha$ -D-mannose

The side-chains of residues Asp54, Gln133, Asn135, Asp140 and the main chain amides of Phe1 and Asp47 participate in a network of H-bonding interactions with exquisite selectivity for the hydroxyl group stereochemistry of  $\alpha$ -D-mannose (Fig. 4A). Minor changes to  $\alpha$ -D-mannose, results in attenuation of, or complete loss of binding affinity. Shown in Figure 2c [39], surface-plasmon resonance (SPR) was used to determine thermodynamic  $K_D$  values for different sugars. It was found that a single configuration change, such as changing the 2-hydroxyl group stereochemistry (D-glucose), or removal of this hydroxyl group, resulted in depletion of FimH binding affinity. Only the five-membered ring sugar, fructose, which has an axial 2-hydroxyl group, could retain some weak FimH binding.

In addition to the direct residue interactions, several water-mediated hydrogen bonds are present between the mannose hydroxyls and the side-chain of Gln133 and the backbone amide of Phe1. Structural discrimination for FimH ligand recognition is also apparent when comparing  $\alpha$ -(axial anomeric hydroxyl) to  $\beta$ - (equatorial anomeric hydroxyl) D-mannose. Only the  $\alpha$ -anomer capable of participating in the water-mediated hydrogen bonds to Asn138 and Asp140 (Fig. 4A). The binding pocket exclusively binds tightly to this anomeric orientation, showing almost no affinity for the  $\beta$ -anomer. Importantly, the key amino-acid residues (Phe1, Asn46, Asp47, Asp54, Gln133, Asn135, Asp140 and Phe142) which encompass the FimH mannose-binding pocket have been found to be invariant throughout all strains of *E. coli*, and mutation of these individual key residues results in a loss of mannose binding and diminished virulence [75, 77].

## 4.2. The 'Tyrosine gate': Hydrophobic surface outside the mannose binding pocket

In addition to mannose sugar binding, a series of equally important molecular interactions take place surrounding the polar sugar recognition pocket. The natural receptors for the FimH lectin contain large, branched, high mannan oligosaccharides, such as oligomannose-3, that terminate the numerous N-glycosylated proteins, which coat the urinary tract [78]. By screening both synthetic oligomannosides, and those isolated from the urine of patients with glycoprotein catabolism disease, it was found that FimH binds with great affinity to a particular sequence of mannose subunits found within the largest high-mannose glycan, oligomannose-9 [26] (Fig. 2b) The oligomannose-5 and oligomannose-3 displayed the highest binding affinities, with  $K_D$  values of 12 nM and 18 nM, respectively [79]. These oligomannosides bind approximately 100-200 times stronger than a single  $\alpha$ -D-mannose monomer. A similar increase in binding affinity (relative to  $\alpha$ -D-mannose), could also be achieved with simple aryl [26, 28] and alkyl [39] mannoside monomers (Fig. 2a). This was a key discovery that has enabled the development of more potent inhibitors through structure based drug design of monovalent FimH mannoside antagonists. When comparing the FimH-bound structures of butyl  $\alpha$ -D-mannoside [39] and oligomannose-3 [76] (Fig. 3A), several important hydrophobic interactions were identified outside the mannose-binding pocket.

Together, the hydrophobic support residues (Phe1, Ile13, Phe142) and 'tyrosine gate' residues (Tyr48, Ile52, Tyr137) form a hydrophobic ridge surrounding the polar binding pocket, with Thr51 extending further out along a hydrophobic groove. Ligand entry into the sugar pocket is framed by the 'tyrosine gate' residues, which also line the hydrophobic groove [80]. Key  $\pi$ -stacking and van der Waals interactions occur within this flexible gate region, and it has been demonstrated that the binding affinity of a mannoside can be largely affected by the ability of the aglycone to orient properly within the tyrosine gate [81]. The flexibility of the gate is due to the dynamic ability of Tyr48 to rotate between three positions: an open-gate configuration, where the residue is positioned toward Asp47; a closed-gate configuration, where Tyr48 is aligned towards the Thr51; or spatially somewhere between the two positions, in a half-open-gate configuration (Fig. 4B) [80]. In its resting state, the tyrosine gate awaits a mannoside ligand in its lowest energy, open position. However, upon binding, Tyr48 can shift in order to minimize the Gibbs free energy ( $\Delta G$ ) of the complexed aglycone [80-81]. For instance, oligomannose-3, extends outward from the binding pocket [76], where it is more energetically favorable for the tyrosine gate to remain in the open state, positioning the oligomannose-3 in the 'in-docking' binding mode (Fig. 3A). However, in the case of other ligands, such as with the sterically rigid 1,4-biaryl aglycones (Fig. 3B), Tyr48 shifts to a closed configuration and the aglycone is positioned outside of the tyrosine gate, in an 'out-docking' binding mode, with the biaryl group forming strong  $\pi$ -stacking interactions with the opposite side of aromatic ring of Tyr48 [37, 40]. Other docking modes are possible which alter the spatial orientation of Tyr48 to achieve maximal  $\pi$ -stacking and binding to FimH (Fig 4B). Further, it was recently reported that a FimH Y48A mutation allows for ligand binding but the Y137A mutant relaxes the gate prior to binding, resulting in a dramatic loss of binding affinity and specificity [82].

### 4.3. H-bonding interactions with the Arg98-Glu50 salt bridge and Tyr48

In the first report of biphenyl mannosides (Table 2) [37, 40], H-bond acceptors on the biphenyl B-ring were found to have increased FimH potency, relative to those without. To explain this result, the first co-crystal structure of a biphenyl mannoside **6** with FimH was solved by the Washington University team [37], revealing for the first time the ‘out-docking’ binding mode (Fig. 3B and 5). In this mode, an H-bonding interaction takes place between the salt bridge of Arg98 and Glu50, which resides just adjacent to the ‘tyrosine gate,’ and the ester carbonyl on the *meta*-position of the B-ring. Another X-ray structure [38], of a mannoside **16** bearing a methyl sulfonamide substituent in the B-ring *para* position (Fig. 5), forms a water-mediated H-bond to the hydroxyl group of Tyr48.

### 4.4 Proximal ortho-pocket accessible to biaryl A-ring substituents

In the earliest report of an aryl mannoside FimH ligand [28], a potency increase was observed upon the addition of an *ortho*-chloro group to para-nitrophenyl  $\alpha$ -D-mannoside. This key structure-activity relationship (SAR) remained largely ignored until 2006, when Sperling *et. al.* [83] investigated this *ortho*-chloro effect through molecular modeling. They predicted that the potency increase was a result of the fit of the *ortho*-substituent into a small depression in the hydrophobic ridge, just adjacent to the sugar binding pocket, as noted with biphenyl mannoside **15** (Fig. 5). Most mannosides reported thereafter incorporate a small *ortho* substituent (such as Cl, CF<sub>3</sub>, or CH<sub>3</sub>) into their aryl mannosides [32, 37, 40-41, 84]. Two different X-ray structures of *ortho*-substituted biaryl mannosides (**15** [45-46] and **20** [38]) were reported at the same time, confirming this small pocket (defined by residues Ile52, Tyr137, and Asn138) was indeed bound by the *ortho* substituent. It was found that *ortho*-substitution on the A-ring, shifts the torsional angle between the A-B phenyl rings [32], as seen in the overlay of *ortho*-methylated mannoside **15** versus unsubstituted biphenyls **6** and **16** (Fig. 5) [45-46], and that this change in ring conformation creates better  $\pi$ -stacking interactions between the B-ring and Tyr48 of the tyrosine gate. The combined effect of the latter, coupled with the increased van der Waals contacts imparted by the *ortho*-substituent, is responsible for the significantly enhanced FimH binding affinity.

## 5. X-ray structure guided design of monovalent, O-mannoside FimH ligands

In 1987, Firon and Sharon published on the first synthetic mannosides as FimH ligands [27-28]. The activity of these initial mannosides, exemplified by *p*-nitro-*o*-chlorophenyl  $\alpha$ -D-mannoside (pNPoCIP $\alpha$ Man), was comparable to known oligosaccharide isolates, such as the Man $\alpha$ 1-3Man $\beta$ 1-4GlcNAc trisaccharide subunit of oligomannose-3, in both an agglutination assay and a competitive binding assay (Fig. 1) [85]. While this discovery introduced the potential of small-molecular weight FimH antagonists, it wasn't until over a decade later [39, 75-76] that the field of rational ligand design of FimH antagonists began, prompted by the X-ray structures of D-mannose, oligomannose-3 and *n*-butyl  $\alpha$ -mannoside. These initial structures helped to elucidate key interactions of the ligand with the FimH hydrophobic residues inside and outside of the polar mannoside-binding pocket (Fig. 4A), allowing for a structure-guided approach to optimizing monovalent FimH antagonists for enhanced binding affinity.

## 5.1. Design and structure activity relationships (SAR) of alkyl and aryl mannosides

Using a surface-plasmon resonance (SPR) assay, several *n*-alkyl mannosides (*n*=1-8) and aryl mannosides (PNP $\alpha$ Man and MeUmb $\alpha$ Man) [28] were tested for their binding affinity to FimH (Fig. 2a) [39]. These data revealed that increased alkyl chain length correlated well with higher affinity, with *n*-hexyl and *n*-heptyl mannosides exhibiting the strongest binding with a  $K_D$  of 10 nM and 5 nM, respectively. Surprisingly, these mannosides displayed better affinity than the aryl mannosides. The increased affinity was attributed to increased van der Waals interactions within both the hydrophobic groove and tyrosine gate regions. However, alkyl mannosides larger than heptyl were found to be less potent, as the alkyl chain extends beyond the hydrophobic region into a more solvent exposed area.

**5.1.1. Squarate and propynyl phenyl mannosides**—Ernst [86] and Lindhorst [83, 87] designed mannoside ligands that possess a squarate (cyclobutene-based) B-ring, attached at the *para* position of a phenyl mannoside *via* an amide bond. This aglycone was predicted to increase van der Waals contact within the hydrophobic groove. While these analogs showed increased activity in the ELISA assay with an RIP of 1800 and 6900 for **1** and **2**, respectively (Fig. 6), attempts to lengthen the aglycone using a glycine or tyrosine linker, resulted in lower activity. Bouckaert also explored extended phenyl A-ring derivatives, containing either a *para*-methoxypropynyl or -hydroxypropynyl substituent [80-81] but found these derivatives had lower binding affinities to FimH than HM by SPR.

**5.1.2. Effect of ring substitution on phenyl mannoside potency**—The crystal structure of oligomannose-3 [76] revealed the tyrosine gate region had flexibility to accommodate mannoside aglycones in either an ‘open’ or ‘closed-gate’ configuration (Fig. 3A and 4B). This finding instigated an in-depth exploration of aryl mannosides, to introduce  $\pi$ -stacking interactions with Tyr48 and Tyr137 and improve FimH binding affinity. Initial studies were reported by Han, et. al. [37] who systematically investigated a series of monosubstituted and disubstituted phenyl mannosides, evaluating the effects of position (*ortho*, *meta*, *para*) and electronic properties (electron withdrawing *vs.* donating) on binding affinity in a FP binding assay and potency in the HAI assay. In general, *ortho*- and *meta*-substituents were found to be more potent than their *para*-substituted matched pairs. The reported HAI titers were typically in the low  $\mu$ M range, with the most potent 3,5-diester analog **3** reaching 2  $\mu$ M (Fig. 6). For comparison, the HAI of  $\alpha$ MM is >1 mM, and PNP $\alpha$ Man is 31  $\mu$ M. The large increase in potency of the di-substituted ring *vs.* the mono-substituted mannoside **4** (HAI = 6  $\mu$ M) might be explained by decreased electron density in the aryl ring caused by two electron withdrawing groups, thus increasing the  $\pi$ -stacking with Tyr137.

**5.1.3. Benzyl and extended alkyl linkers**—Adding alkyl groups between the mannose ring and the phenyl ring of phenyl mannoside **5** (HAI = 30  $\mu$ M) [32, 37] resulted in decreased potency, making the phenyl mannosides optimal for further optimization. Mannosides possessing propynyl or acetamido linkers, such as **18b** (Fig. 5) were explored by Bouckaert *et. al.* [80-81] to increase binding within the tyrosine gate, but were significantly less potent than HM ( $K_D$  range of 59 nM to 4.2  $\mu$ M).

## 5.2. Biphenyl, biaryl and other mannosides with multi-ring aglycones

**5.2.1. SAR of B-ring placement and substitution on potency**—Molecular docking studies on mono-aryl mannosides, suggested that that further improvements in binding affinity could be achieved through the addition of a second aryl ring (B-ring), to increase hydrophobic and  $\pi$ -stacking interactions within the tyrosine gate region. Accordingly, in papers by both Klein [32] and Han [37], they developed extensive libraries of biphenyl mannoside inhibitors, wherein a wide variety of A, B-ring configurations and substituents were evaluated for SAR (Table 2). Overwhelmingly, the most effective (binding and functional activity) ring systems have the Bring off the *para* position of the A-ring.

Using this scaffold, Janetka and colleagues [37] identified an early lead that contained an ester on the *meta* position of the B-ring (**6**; HAI = 1  $\mu$ M (15-fold better than HM)). Unlike oligomannose-3, the biphenyl was found to bind to FimH with a closed tyrosine gate in an ‘outdocking’ binding mode, forming  $\pi$ -stacking interactions with the opposite side of Tyr48. The ester carbonyl forms a H-bond with the Arg98-Glu50 salt bridge for enhanced affinity. The importance of this interaction was validated through analog synthesis where it was found that *ortho*- and *para*-substituted analogs, which can't participate in this H-bond, lost activity. Subsequent SAR studies revealed that the 3,5-disubstituted ester biphenyl mannoside **7** had a marked 100-fold increase in potency (HAI = 0.15  $\mu$ M), presumably due to improved  $\pi$ -stacking with Tyr48.

Soon after, *para*-substituted derivatives were reported by the Ernst group [32], with a methyl ester **8** or carboxylic acid **9**, having the best potency in an anti-aggregation assay and binding assay (**8**; IC<sub>50</sub> = 10.4 nM). Docking studies predicted a ‘out-docking’ binding mode for **8**, wherein the biphenyl moiety is oriented outside the tyrosine gate [40]. Another series of analogs contained different linkers to the biphenyl or alternate ring systems where the B-ring is attached at different A-ring positions (Fig. 6). These were designed to bind in the more energetically favorable ‘in-docking’ binding mode. However, the most potent derivative **10** only showed an IC<sub>50</sub> = 86 nM in a bacterial binding assay [40].

**5.2.2. SAR of A-ring ortho-substitution**—The studies discussed in the previous section [32, 40-41, 84] also elucidated that addition of an *ortho* substituent on the phenyl A-ring had a powerful effect on biphenyl inhibitor potency. While *ortho*-substitution increased potency with phenyl mannoside derivatives [28, 37, 83], its impact was more profound when incorporated into the biphenyl analogs, thus becoming an indispensable component of future mannosides. Interestingly, FimH binding affinity was found to improve with the increased van der Waals volume of spherical *ortho*-substituents, finding trifluoromethyl, methyl, and chloro substituents optimal relative to methoxy, cyano, cyclopropyl and fluorine [40-41]. For example [41], the potency of **6** only increased slightly *via* addition of an *ortho*-fluorine (**11**; HAI = 0.75  $\mu$ M), whereas a more significant increase occurred with the larger and more polarizable *ortho*-chlorine substituent (**12**; HAI = 0.03  $\mu$ M). Excitingly, these analogs were demonstrated to disrupt bacterial biofilm formation, with IC<sub>50</sub> values in an unprecedented low nM range. Furthermore, some compounds had K<sub>D</sub> values which were too low to measure using the BLI binding assay, due to extremely slow off-rates. In the DSF assay, the melting point change of a FimHmannoside complex, a measure of the mannoside binding

affinity, was found to correlate well with the HAI titers. Ernst and coworkers also reported [40] increases in potency with *ortho*-chloro-substituted derivatives, such as **13** and **14** (IC<sub>50</sub> = 4.8 nM, 6.7 nM), relative to the unsubstituted analogs **8** and **9** (IC<sub>50</sub> = 10.4 nM, 17.1 nM).

A high resolution structure of *ortho*-methyl mannoside **15** (Fig. 5) [46], uncovered that the increase in affinity, may arise from a shift in the conformation of the biphenyl ring, allowing for improved interactions in the hydrophobic pocket [46]. In this structure, the B-ring amide no longer forms a direct interaction with the salt bridge like **6** (Fig. 3B and 5), but unexpectedly forms a water-mediated H-bond to the Tyr48 hydroxyl group. In a similar fashion, the X-ray structure of **16** [38], also shows that the *para*-sulfonamide B-ring substituent forms a direct H-bond to Tyr48. Taken together, these results show that minor variations in both A-ring and B-ring substitution patterns affect the biphenyl ring conformations as well as the ability of substituents to form electrostatic or H-bonding interactions with the salt bridge and Tyr48 of the tyrosine gate of FimH.

**5.2.3. A-ring variations: Triazoles and other heterocycles**—The use of ‘click’ chemistry methodology has been used to construct a library of unique biaryl ring systems with a triazole A-ring.[88] These analogs were thought to have extra conformationally flexibility, allowing for improved interaction with the tyrosine gate region. In contrast to the ‘out-docking’ mode displayed with biphenyl mannosides, they were designed to bind in a lower energy ‘in-docking mode,’ to strengthen FimH binding. Unfortunately, this series only retained minimal activity, with the most promising 4-pyridyl derivative **17**, having an IC<sub>50</sub> = 0.07 μM (Fig. 6). *N*-phenyl-substituted hydroxypyridinone mannosides have also been explored as FimH ligands [89] but the most active example **18a** has a poor HAI = 625 μM.

**5.2.4. Spaced-biaryl configuration of aglycone**—Another approach to unique biaryl systems, relied on a branched 1,3-diaminopropanol or glycerol linker terminated by two aryl moieties [90]. Molecular modeling predicted an open tyrosine gate was best able to accommodate these derivatives, having one aryl moiety residing within the tyrosine gate in an ‘in-docking’ fashion, and the other located outside the gate, interacting with Phe142 and Ile13. Despite the modeling, this did not give an increase in activity, as seen with **13e**. There are also several reports of other biaryl aglycones that contain a spacer between the A and B phenyl rings. For example, Lindhorst created a series of photoactivatable diazo-linked A and B phenyl rings [91-92], and Ernst synthesized mannosides with amide linked A-B rings [86].

### 5.3. Other considerations in ligand design: Conformational variability of FimH

Several research groups have demonstrated the existence of conformational equilibria in FimH, which vary according to FimH sequence, ligation state, and physiochemical properties such as fluid flow. Most recently, the Hultgren group [53] described an allosteric, ensemble-based model for mannose binding by FimH, in which FimH in solution adopts a pre-existing two-state equilibrium of a low-affinity T-state conformation and multiple high-affinity R-state conformations that both engage mannose through distinct binding modes. Through this work, it was demonstrated that a balanced equilibrium between T and R states in FimH confers “moderate” mannose-binding affinity, which is optimal for bladder colonization by *E. coli* during UTI. Positively selected residues in FimH can skew this



equilibrium toward the T or R state, thereby modulating mannose binding affinity in either direction and reducing pathogenicity. Furthermore, ligand or mannoside binding to FimH shifts its pre-existing equilibrium toward the high-affinity R state while occluding the mannose binding pocket and inhibiting host-pathogen interactions. Reports from several other groups [54-55, 93-94] postulate that urine flow in the bladder kinetically selects the rapidly-associating low-affinity conformation of FimH for receptor binding and that shear stress converts this bound low-affinity conformation to a bound high-affinity conformation of FimH. While the *in vivo* relevance of shear stress to human UTI remains unclear, these structural studies suggest that mannosides can in fact target both the low-affinity T state in addition to the high-affinity R state.

These studies are based on only a few FimH mannoside ligands[54], but the data suggests that individual mannosides can bind to these different states with significantly different affinities, while others bind with equal affinity to both the high affinity R and low affinity T conformations. It has also been shown that mannosides can bind with different affinities under “flow” or “non-flow” conditions as determined from *in vitro* assays [95-97]. Taken together, further studies are necessary to (a) determine the role of shear stress on pathogenicity *in vivo* and (b) assess the SAR and selectivity of many diverse mannosides toward these two conformations.

## 6. Medicinal chemistry lead optimization of drug-like FimH mannoside antagonists

### 6.1. Metabolic stability of the glycoside bond and aglycone

Carbohydrates and smaller glycosides are susceptible to hydrolysis at low pH in the stomach and to enzymatic degradation by glycosidases. Relevant to this review, synthetic mannosides with unnatural aglycone fall into this class of compounds and thus have this potential liability. For example [62], an analysis of urine after oral dosing of compound **6** in mice, showed the presence of both the parent compound unchanged and varying amounts of the hydrolyzed aglycone (phenol) depending on the dose. Furthermore, carboxylate functional groups, such as the methyl ester of compound **6** or amide **15**, can be metabolized by carboxylesterases and amidases, respectively [32]. To overcome these potential liabilities, alternatives to the *O*-glycosidic anomeric bond and enzymatically stable bioisosteres of the ester or amide present in early potent mannosides, have been explored at length.

### 6.2. Structure property relationships: LogD, solubility and cell permeability

To maximize absorption in the gut, decent solubility and cell membrane permeability in the intestinal tract are necessary. The hydrophobic nature of the synthetic aglycones can significantly diminish the inherent solubility afforded by the D-mannose sugar ring. To illustrate this point, compounds like **7** [37] and **8** [32] have low solubility and are not useful for oral dosing. Replacement of the ester of **7** with a methyl amide (**19**) retains potency but greatly enhances compound stability and solubility, resulting in improved oral *in vivo* efficacy when tested in animal models of UTI [62]. Increasing aqueous solubility usually equates with higher polarity (lower LogD) and can weaken a compounds ability to cross cell membranes through passive diffusion in the intestine, which requires some degree of

lipophilicity, shown to be optimal with mannosides having a  $\text{LogD} > 2$  [84]. Therefore, a balance must be found between these two opposing parameters, to design mannosides having a high enough  $\text{LogD}$  and solubility to be an orally bioavailable drug [98]. Prediction of membrane permeability in the intestine, can be obtained by using a parallel artificial membrane permeability assay (PAMPA), the colonic adenocarcinoma (Caco-2) cell monolayer assay, or an MDR1-MDCK permeability assay capable of assessing efflux as well [98].

### 6.3. Strategies to increase half-life and renal clearance

Due to the nature of a UTI, where the bacteria reside in the urine and bladder, an extended half-life and high renal clearance of a drug is desired. Three parameters which can adversely affect a mannosides half-life, are metabolism, a low volume of distribution ( $V_{\text{dss}}$ ) and a high plasma clearance rate (Cl). Efforts to improve half-life have mainly been focused on increasing cell permeability and metabolic stability. Polar compounds typically exhibit high renal clearance [99], which is desired for mannosides as drugs for UTI. However, this rapid elimination of drug requires frequent dosing to maintain maximal therapeutic benefit. A moderate increase in  $\text{LogD}$  can elevate tubular reabsorption, resulting in a slower excretion of the drug. Another parameter which can directly affect renal clearance of mannosides is the plasma protein binding (PPB). This protein binding sequesters drug from binding to its target, in this case FimH, and compound must dissociate before it excreted in the urine. Ernst reported that moderate protein binders ( $f_b \approx 65\%$ ) would be susceptible to rapid clearance, whereas compounds with a PPB  $f_b \approx 90\%$  were more likely to experience sustained plasma concentrations. For example, *para*-cyano derivative **20** ( $f_b \approx 89\%$ ), was found to retain therapeutic mannoside levels in the urine over a prolonged period after oral dosing (Table 3).

### 6.4. Aglycone modifications: effects on physicochemical and PK properties

**6.4.1. Heteroaryl B-rings (isoquinolines and isoquinolones)**—The incorporation of heterocycles offers a nice framework to manipulate the physicochemical properties of compounds, such as lipophilicity, solubility, stability and pKa, thereby promoting changes in both ligand binding affinity and pharmacokinetic properties. As an example of this strategy in FimH ligand design, Janetka and colleagues [41] evaluated a small set of B-ring heterocycles, which retained the beneficial H-bonding capabilities and potency of the biphenyl mannosides (Table 2). These heterocycles were designed as bioisosteres of the amide functionality with increased stability to amidases and higher  $\text{LogD}$ , leading to mannosides with improved physical and PK properties (Table 3). The SAR derived from this mannoside library (Table 4) was crucial to designing new mannosides with improved oral bioavailability. From this series, isoquinolone **21** and isoquinoline **22** emerged as new lead compounds.

In a subsequent study [46], the A-ring *ortho*-substitution was also incorporated, to yield isoquinolone **23** (HAI = 30 nM) and **24** (HAI = 62 nM), displaying an enhancement in activity relative to acyclic amide derivative **25**. Most importantly, **23** was shown to reduce UPEC CFUs 10,000-fold in the chronic mouse model of UTI (p.o., 50 mg/kg), or 10-fold better over **25** and **15**. PK analysis (Table 5) revealed that the improved efficacy is likely

attributed to the increased bioavailability (F) of **23**, relative to **25** (7.0% vs. 1.4%) and tissue exposure ( $V_{dss}$ ), which could explain the corresponding increased rate of plasma clearance. Following this positive result, the group investigated the effect of pKa on half-life, clearance, tissue exposure, and oral bioavailability [46], with a series of N-substituted isoquinolones based on **23**. These modifications resulted in a significant increase in potency, with several examples achieving single digit nanomolar potency (e.g. 3-pyridylacetamide **26**, HAI = 1 nM; and biofilm  $IC_{50}$  = 18 nM). On the other hand, the substitutions had a negative effect on oral bioavailability, with only the 3-pyridylcarboxamide **27** showing measurable *in vivo* efficacy. The reason for the lack of gut permeability remains unclear but it could be due to the lower LogD (limiting passive diffusion), increased metabolism of the glycosidic bond, and/or efflux.

**6.4.2. N-linked indoles and indolines**—Indole B-ring derivatives [84], which are linked to the mannoside A-ring through the nitrogen were reported in 2012 (Table 4). These were designed to have improved fit within the FimH binding pocket as well as a better PK/PD profile. It was determined that the optimum mannoside profile should have a LogD < 2, a PAMPA value of > -6.0, and exhibit PPB > 95%. Using these parameters as a guide, three compounds were selected for *in vivo* studies, including *ortho*-chloro indole **28** ( $IC_{50}$  = 14.9 nM), nitroindoline **29** ( $IC_{50}$  = 20 nM) and *ortho*-chloro nitroindoline **30** ( $IC_{50}$  = 2.4 nM), which was selected for its increased binding, relative to the other analogs. In this study, mannoside **29** exhibited the best renal elimination profile (Table 5) when dosed IV at 1 mg/kg in mice, where the dose could be decreased 50-fold, relative to **14**, with good compound exposure over 8h. In a follow-up study, UTI89 bacteria infected C3H/HeN mice treated with **29** (i.v. 1 mg/kg), showed a 4-fold improvement in reducing bladder bacterial CFUs, relative to **14** (i.v. 50 mg/kg), comparable to ciprofloxacin. However due to poor aqueous solubility, **48a** does not allow for oral administration.

**6.4.3. Evaluation of B-ring substituents as determinants of PK**—In 2015 [38], biphenyl mannosides were revisited to identify a FimH antagonist with a more balanced solubility/permeability profile suitable for oral administration. Starting from lead compound **8**, a series of bioisosteric replacements were made to the B-ring *para*-carboxylate. This work produced a small library of compounds from which **31** (*p*-morpholineamide), **16** (*p*-sulfonamide), and **20** (*p*-cyano) emerged as the top candidates for *in vivo* studies. These mannosides possess their optimal PK profile due to high renal excretion (**31** due to its low LogD and PPB), or **20** and **16** which are expected to undergo slower renal elimination, because of their higher LogD and PPB. Mannoside **20** has a 3-fold increase in FimH binding affinity in the FP assay (**20**,  $K_D$  = < 1 nM) relative to **8**. Excitingly, the solubility of **20** was nicely improved over nitroindoline **29**. An X-ray structure of **20** (PDB code: **4CST**) is similar to **16** (Fig. 5) where the biphenyl exists in an ‘out-docking’ orientation. In mouse PK, **20** excelled over other analogs, displaying prolonged compound exposure in the urine out to 8h (Table 5). In a prophylactic mouse model of UTI, **20** reduced CFUs 1000-fold (p.o. 10 mg/kg), showing some benefit over ciprofloxacin.

## 6.5. Exploration of alternate O-glycosidic bond linkers: Addressing metabolic stability

To improve the metabolic stability of *O*-mannosides, alternative glycosidic bonds and linkers have been extensively investigated. This work, summarized in Figure 7, has led to mannosides with improved solubility and other physicochemical properties, but has also created some undesired effects which will be discussed at length. These studies represent the most substantial advances in the development of FimH antagonists, suitable as drugs for both UTI and CD patients.

**6.5.1. Thiazolymannosides ‘Tazmans’—TazMans (thiazolymannosides)** were designed by Gouin and Bouckaert [35-36] as inhibitors of FimH function attributed to the attachment and colonization of AIEC in the intestinal mucosa of Crohn's disease (CD) patients. Unlike UTIs, where the bladder is the site of infection, necessitating oral bioavailability; target AIEC bacteria are localized in the intestinal tract, only requiring mannosides with good solubility and stability in the gut. Accordingly, the unique class of mannosides were designed for better aqueous solubility. The first round of TazMans consisted of an *N*-linked aminothiazole A-ring, which was attached to various functional groups through a ketone linker (Fig. 7). In general, heteroaryl ring groups were among the best, like tri-aryl analog **32**, which was 5-fold more potent than HM in an HAI assay, and 100-fold more effective at blocking LF82 bacterial adhesion to intestinal epithelial T84 cells *in vitro*. **32** was also shown to abrogate bacterial attachment to colonic tissue from CEABAC10 mice *ex vivo*. While promising, these TazMans were unstable at low pH, isomerizing into the inactive  $\beta$ -mannoside isomers. Therefore, a second round of derivatives were synthesized, having the nitrogen atom replaced with *O*-, *S*-, and *C*-based linkers. The new derivatives were more stable, but they did not reach the activity levels seen from the *N*-linked analogs. To explain this, it was proposed that the anomeric nitrogen atom was being stabilized by a water-mediated hydrogen bond to FimH. Rational design attempts placing the thiazolyl A-ring closer to the Tyr48 residue to increase  $\pi$ -stacking by adding methylene units to the linker were unsuccessful.

**6.5.2. C-alkyl and thioalkyl glycoside linkers with improved stability**—In another series targeting AIEC bacteria in CD, Gouin[22] designed a sulfur and carbon-linked heptyl *O*-mannoside (HM) derivatives (Fig. 7). Direct comparison of matched pairs in the ELLSA binding assay showed the *O*-mannosides were noticeably more potent than the *S*-linked and *C*-linked pairs. However, their FimH binding affinities ( $IC_{50}$  = 118 nM to 203 nM) were in a similar range to that of HM ( $IC_{50}$  = 160 nM). *C*-linked mannoside **33** was selected for *in vivo* studies based on its *in vitro* activity ( $IC_{50}$  = 203 nM) and ability to disrupt a pre-established LF82 bacterial colonization of T84 intestinal epithelial cells. In the mouse model of Crohn's Disease, **33** (p.o. 10 mg/kg) decreased LF82 levels by 2-log units in the feces, while also eliminating all AIEC from the ileum.

**6.5.3. C-alkyl and alkenyl linked aromatic aglycones**—Bouckaert and colleagues [100] reported on another series of *C*-linked biphenyl mannosides. However, only three analogs (Fig. 7) were synthesized with no report of biological activity. Co-crystal structures of the three analogs bound to the lectin domain of FimH highlighted that the *cis*-configured alkenyl-linker **34**, accommodates the aglycone portion within an open tyrosine gate

configuration, whereas the trans-configured alkenyl-linker **35** binds in the closed tyrosine gate, both in the ‘in-docking’ mode. With regards to the more flexible propyl-linked naphthalene aglycone **36**, the saturated alkane allowed for much rotational freedom, resulting in a binding mode wherein the aglycone was not well stabilized. This paper highlights a water-mediated H-bond to FimH Asp140 seen with *N*- and *O*-linked derivatives, but not possible with the *C*-linked mannosides, leading to diminished binding affinity.

#### 6.5.4. R-hydroxymethylene C-linked mannosides with improved stability and potency

—A large step forward in the development of optimized *C*-linked mannosides, came with discovery of the *R*-hydroxymethylene linker [45]. Replacing the anomeric oxygen with this novel linker, yielded a potency increase of up to 8-fold, relative to the *O*-mannoside matched pairs. In a computational docking model, the *R*-hydroxyl group of the more potent *meta*-amide analog **37** (HAI = 31 nM), participates in a tri-dentate water-mediated hydrogen bond to Asn135 and Asp140 [100]. In contrast, the *S*-hydroxymethylene linked analog **38** (HAI = 6  $\mu$ M) is not able to participate in this hydrogen bonding network. Consistent with this docking model and the X-ray structure of simple alkyl *C*-mannosides, the methylene-linked derivative **39** (HAI = 2  $\mu$ M), suffers from attenuated potency due to its inability to access the water-mediated H-bond. Amazingly, *C*-mannoside **37** maintained a concentration in the mouse urine at a 100-fold higher level relative to **25**, at 8h post oral dosing at 50 mg/kg (Table 5). This can be rationalized from increased stability and/or enhanced renal excretion. The optimized *R*-hydroxymethylene linker was utilized to construct a set of heterocyclic biaryl *C*-mannosides, based isoquinolone *O*-mannoside **23**. Exemplified by **40** (Fig. 7), these optimized *C*-mannosides are significantly more potent (HAI = 6-8 nM, and biofilm IC<sub>50</sub> = 30-40 nM). When tested in an *in vivo* acute prophylactic mouse model of UTI, orally dosed at 25 mg/kg, **40** showed a 2-log reduction in bacterial CFUs in the bladder (100-fold increase over **23**).

**6.5.5. Direct linked aryl A-ring**—In a 2013 patent application [101], Vertex claimed several hundred different *C*-mannosides where a biaryl aglycone is directly attached to the anomeric carbon of D-mannose. While no rationale was explicitly stated within the application, it can be implied they were designed with metabolic stability in mind. Most examples had aglycones with either biphenyl, heterobiaryl, or a phenyl A-ring with either an alkyl, amide or ether-based linker connecting it to a phenyl B-ring (Fig. 7).

**6.5.6. C-linked ‘disaccharides’**—Mannose disaccharides which are connected *via* a non-hydrolyzable  $\alpha$ 1-3 carbon-carbon linkage have also been reported [102]. These compounds, exemplified by **41** and **42** (Fig. 7), were specifically designed for the treatment of CD, as their increased hydrophilicity and molecular weight will limit oral bioavailability. The reducing end of this disaccharide likely interacts with FimH akin to the terminal Man $\alpha$ 1-3-linked sugar unit of oligomannose-3, where the second mannose residue could function as an extension of the mannoside aglycone.

## 7. Other approaches to FimH antagonists based on D-mannose

### 7.1. Modifications to the D-mannose sugar-ring

While the most attention on FimH antagonists has been aimed at altering the linker and aglycone, there have been efforts focused on manipulating the mannose core. The mannose-binding pocket demands strict stereochemical recognition, so any modification to the sugar-ring must be carefully designed. To this end, Vertex employed simple changes such as, fluorination (**43**), alkylation (**44**), and an anomeric-fused spiroketal ring systems (**45**) [103]. Many of these derivatives were combined with previously reported aglycones. Overall, these changes elicited a wide range of activities ( $IC_{50} = 10 \mu\text{M}$  to 8.6 mM) in the bacterial binding assay with LF82 AIEC (Fig. 7).

### 7.2. Mannoside prodrugs of the D-mannose ring

*O*-mannosides have low oral bioavailability caused by low stability, solubility or cell membrane permeability. *C*-mannosides have solved the stability issue but still suffer from low bioavailability due to lowered LogD. As a strategy to increase oral bioavailability, mannoside prodrugs have been pursued.

**7.2.1. Acylated D-mannose derivatives (ester prodrugs)**—Janetka and Ernst [45, 104] both explored the use of ester-prodrugs to increase the oral efficacy of lead mannosides. For example, the lipophilic tetra-acetate *meta*-amide **25a** [45] (Fig. 8) showed a 20-fold increase in the concentration of active drug **25** in the urine (6h, post oral dosing). Thus, **25a** showed significantly better efficacy at reducing bacterial colonies. To optimize the renal excretion profiles [104], the structural relationship between the type of ester prodrug and its rate of metabolic hydrolysis and membrane permeability were investigated. When compared to parent compound *para*-methylsulfonyl mannoside **16a**, the entire library of 6-O-monoacylated ester prodrugs (Fig. 8) showed an improvement in predicted permeability (Table 3) with the straight-chain prodrugs (ex. **16b**) having higher aqueous solubility than the branched derivatives (ex. **16c**). In addition, all prodrugs showed good stability under physiological and acidic pH in the stomach and GI tract. Enzymatic hydrolysis of these prodrug esters was shown to take place predominantly by the human carboxylesterase isotype 2 (hCE2), which is a major carboxylesterase in both the liver and small intestine. When tested for prodrug activation rates, those with shorter or branched chains exhibited better stability than the longer aliphatic chains. While efficient cleavage of the prodrug is desired prior to absorption, premature hydrolysis by hCE2 could preclude absorption altogether, which still needs to be confirmed *in vivo*.

**7.2.2. Phosphorylated prodrugs of mannosides**—Phosphate prodrugs have also been employed for mannosides [105] that have good membrane permeability, such as *para*-cyano **20** and nitroindoline **29**, but can't be absorbed in the gut due to poor aqueous solubility. In one study, it was shown that slow hydrolysis of the phosphate ester was optimal, allowing for maximum absorption of the active drug, at a rate that avoids precipitation. The location of the phosphate produced differing rates of hydrolysis, with the 4-O-phosphate **20a** exhibiting the slowest rate (by alkaline phosphatase in the Caco-2 permeability assay). The increased solubility of the phosphate prodrugs results in higher



concentration gradients across the Caco-2 cells, promoting drug uptake while saturating P-Gp efflux, leading to higher overall absorption. Indeed, when **20a** was tested *in vivo*, the urine AUC of parent drug **20**, was significantly increased.

**7.2.3. Disaccharides of D-mannose**—In a patent application [101], examples of man1-3man disaccharides derivatives possessing C-linked aglycones (Fig. 8) were disclosed by Vertex. We deduce from their structures, that these were purposefully designed as intestinal prodrugs with improved solubility, aimed at the treatment of CD, where oral bioavailability is undesired. Their higher molecular weight and lower LogD is predicted to limit oral bioavailability, while metabolism by gut mannosidases will presumably hydrolyze these disaccharide-based mannosides into the more active C-linked monosaccharide forms.

## 8. Multivalent mannosides: The promise of avidity from multiple mannose rings

### 8.1. Glycodendrimers and glycoconjugates

Prior to the discovery of high affinity monovalent mannosides, much of work in developing inhibitors of FimH bacterial attachment was to tether together multiple D-mannose rings to achieve a potency enhancement due to multivalency or a “clustering effect,” where this inhibitor can bind to multiple bacteria at the same time [106-107]. While this focus has largely been replaced by the rational design of orally bioavailable lower molecular monomeric mannosides, several multivalent mannoside inhibitors have been reported, including glycodendrimers and neoglycoproteins [107-108], CD-based HMs [69, 109-114], glycoclusters [115-116], and others [117-120]. While these have been extensively reviewed previously [121-122], we present select examples of smaller, di- and tri-valent mannosides in the following discussion.

### 8.2. Anomeric-linked di- and trivalent mannosides

Several recent patent applications have disclosed di- and tri-valent mannoside inhibitors of FimH adhesion. Therein, the anomeric centers are either O-linked [103] or C-linked [123] to a central phenyl-based aglycone. Several examples are based on already established mono- and biphenyl aglycone structures, while others are composed of elaborate ring systems. Since no rational design strategies are explicitly stated, only the most potent examples (**46** and **47**) are shown in Figure 8. Interestingly, multiple examples of related divalent mannosides were first reported by Janetka and colleagues in 2010 [37], wherein dimers of biphenyl mannoside **25** were created through use of PEG-linkers of differing lengths to bridge the aglycones. As a representative example, dimer mannoside **49** with a PEG-2 linker between the two B-ring amides, resulted in an impressive 8-fold increase in HAI potency (4-fold per mannose) relative to monomer **25**.

## 9. Conclusions

Small molecule FimH mannosides have now been rationally developed which have good drug-like properties and oral efficacy in preventing and treating UTIs *in vivo*. Mannosides also display activity in animal models of CD.

## 10. Expert Opinion

Early mannoside FimH antagonists were rationally designed by X-ray structure-based ligand design [32, 62], but were subject to enzymatic hydrolysis by mammalian and bacterial mannosidases in the gut and plasma. To design an effective drug for UTI therapy, mannosides need to possess good metabolic stability and half-life, adequate permeability in the gut, and efficient renal clearance to the bladder. This required fine-tuning the mannoside structure to find a balance between both physical and pharmacokinetic properties such as solubility, plasma protein binding, cell membrane permeability and lipophilicity, while retaining potency. During the last 5 years, extensive medicinal chemistry efforts from several laboratories have investigated diverse alteration of mannosides, to identify mannosides optimized for both drug likeness and potency.

These monumental efforts have now resulted in the discovery of potent mannosides with extraordinary diversity that encompass good *in vivo* activity in animal models of UTI or CD. While the several models for UTI are widely accepted to closely duplicate human disease, treatment in the AIEC model in CD preceded the development of acute pathology and an outstanding question is whether FimH antagonists could impact on chronic, long standing disease. Although metabolic stability of mannosides as drugs is key for either application to UTI or CD, the divergence in FimH antagonist drug design is apparent when comparing the different strategies. Monovalent mannosides are preferred in UTI with good intestinal permeability while multimeric forms with limited oral bioavailability are desired for CD.

Enterome licensed the FimH mannoside portfolio from Vertex in early 2016 and has subsequently reported on a 'first-in-class' FimH antagonist, EB8018. Judging from our expert opinion and a presentation by Enterome at the Microbiome Summit in November 2016, we suspect that EB8018 is a divalent mannoside with a covalent bridge between the aglycones of two mannosides. EB8018 entered phase 1 clinical trials just prior to this review in January 2017, to assess safety for the treatment of patients with Crohn's Disease. At the same time, multiple monovalent *O*- and *C*-mannosides holding sufficient metabolic stability, half-life, renal clearance and oral bioavailability have been discovered and are being developed as antivirulence drugs to treat UTI patients.

The startup company, Fimbrion Therapeutics was founded in late 2012, in part to commercialize the FimH mannosides developed by Washington University scientists in Saint Louis. In late 2016, Fimbrion published a press release announcing they were working in a scientific collaboration with GlaxoSmithKline to complete the preclinical lead optimization of orally bioavailable mannosides as new antibiotic-sparing therapy for UTI. While it is uncertain as to the status of the compounds or the exact clinical application of their FimH antagonists [45-46] at this time, it is our opinion, based on the quality of the latest mannosides reported by Fimbrion, that it is expected that human trials in patients will begin within the next two years. Pending the outcome of these trials of first-in-class oral mannoside FimH antagonists in UTI patients, a new era in antibacterial research is upon us. Antibiotic-sparing FimH antagonists for UTI and new drugs targeting other bacterial adhesins and virulence factors for treatment of other Gram negative infections, promise to

provide an exciting and necessary solution to the terrible medical crisis we are now facing with the rise of multidrug (MDR) and now pandrug (PDR) antibiotic resistance.

## Acknowledgments

**Funding:** The authors are funded by a grant from the National Institute of Allergy and Infectious Disease via grant (no. 5R43A1106112-02).

## References

Reference annotations

\* *Of interest*

\*\* *Of considerable interest*

1. Ronald AR, Nicolle LE, Stamm E, et al. Urinary tract infection in adults: research priorities and strategies. *Int J Antimicrob Agents*. 2001; 17(4):343–8. [PubMed: 11295419]
2. Foxman B. Recurring urinary tract infection: incidence and risk factors. *American Journal of Public Health*. 1990; 80(3):331–33. [PubMed: 2305919]
3. Foxman B. Urinary tract infection syndromes: occurrence, recurrence, bacteriology, risk factors, and disease burden. *Infectious Disease Clinics of North America*. 2014; 28(1):1–13. [PubMed: 24484571]
4. Griebing, TL. Urinary tract infection in women. In: Litwin, MS., Saigal, CS., editors. *Urologic Diseases in America*. US Government Printing Office; Washington, DC: 2007. p. 587-620.
5. Sanchez GV, Master RN, Bordon J. Trimethoprim-sulfamethoxazole may no longer be acceptable for the treatment of acute uncomplicated cystitis in the the United States. *Clinical Infectious Diseases*. 2011; 53(3):316–17. [PubMed: 21765092]
6. Karlowsky JA, Hoban DJ, Decorby MR, et al. Fluoroquinolone-resistant urinary isolates of *Escherichia coli* from outpatients are frequently multidrug resistant: results from the North American Urinary Tract Infection Collaborative Alliance–Quinolone Resistance study. *Antimicrob Agents Chemother*. 2006; 50(6):2251–4. [PubMed: 16723598]
7. Zhanel G, Hisanaga T, Laing N, et al. Antibiotic resistance in *Escherichia coli* outpatient urinary isolates: final results from the North American Urinary Tract Infection Collaborative Alliance (NAUTICA). *Int J Antimicrob Ag*. 2006; 27(6):468–75.
8. Schaeffer A. The expanding role of fluoroquinolones. *Disease-a-Month*. 2003; 49(2):129–47. [PubMed: 12601342]
9. Dielubanza E, Schaeffer A. Urinary Tract infections in women. *Medical Clinics of North America*. 2011; 95(1):27–41. [PubMed: 21095409]
10. Cole ST. Who will develop new antibacterial agents? *Philosophical Transactions of the Royal Society, B: Biological Sciences*. 2014; 369(1645):20130430.
11. Nathan C. Fresh approaches to anti-infective therapies. *Sci Transl Med*. 2012; 4(140):140sr2. [PubMed: 22745440]
12. Lee YM, Almqvist F, Hultgren SJ. Targeting virulence for antimicrobial chemotherapy. *Curr Opin Pharmacol*. 2003; 3(5):513–9. [PubMed: 14559097]
13. Rasko DA, Sperandio V. Anti-virulence strategies to combat bacteria-mediated disease. *Nat Rev Drug Discov*. 2010; 9(2):117–28. [PubMed: 20081869]
- 14\*. Garland M, Loscher S, Bogyo M. Chemical strategies to target bacterial virulence. *Chem Rev*. 2017; 117(5):4422–61. Excellent recent review on anti-virulence approaches, other than FimH and adhesins. [PubMed: 28234447]
15. Cozens D, Read RC. Anti-adhesion methods as novel therapeutics for bacterial infections. *Expert Rev Anti Infect Ther*. 2012; 10(12):1457–68. [PubMed: 23253323]
- 16\*. McGann P, Snesrud E, Maybank R, et al. *Escherichia coli* harboring *mcr-1* and *blaCTXM* on a novel IncF plasmid: first report of *mcr-1* in the United States. *Antimicrob Agents Chemother*.

- 2016; 60(7):4420–1. First reported case of a patient bearing a pan-antibiotic resistant UPEC UTI in the US. [PubMed: 27230792]
17. Mediavilla JR, Patrawalla A, Chen L, et al. Colistin- and carbapenem-resistant *Escherichia coli* harboring *mcr-1* and *bla*NDM-5, causing a complicated urinary tract infection in a patient from the United States. *mBio*. 2016; 7(4):e01191–16. [PubMed: 27578755]
  18. Snyder J, Lloyd A, Lockett C, et al. Role of phase variation of type 1 fimbriae in a uropathogenic *Escherichia coli* cystitis isolate during urinary tract infection. *Infect Immun*. 2006; 74(2):1387–93. [PubMed: 16428790]
  19. Wu XR, Sun TT, Medina JJ. In vitro binding of type 1-fimbriated *Escherichia coli* to uroplakins Ia and Ib: relation to urinary tract infections. *Proc Natl Acad Sci USA*. 1996; 93(18):9630–35. [PubMed: 8790381]
  20. Anderson GG, Palermo JJ, Schilling JD, et al. Intracellular bacterial biofilm-like pods in urinary tract infections. *Science*. 2003; 301(5629):105–7. [PubMed: 12843396]
  21. Zhou G, Mo WJ, Sebbel P, et al. Uroplakin Ia is the urothelial receptor for uropathogenic *Escherichia coli*: evidence from in vitro FimH binding. *J Cell Sci*. 2001; 114(Pt 22):4095–103. [PubMed: 11739641]
  - 22\*. Dorta DA, Sivignon A, Chalopin T, et al. The antiadhesive strategy in Crohn's disease: orally active mannosides to decolonize pathogenic *Escherichia coli* from the gut. *Chembiochem*. 2016; 17(10):936–52. Demonstration of *in vivo* efficacy of a FimH antagonist in Crohn's Disease. [PubMed: 26946458]
  - 23\*. Duguid JP, Gillies RR. Fimbriae and adhesive properties in dysentery bacilli. *J Path Bact*. 1957; 74(2):397–411. The first mention of mannose as a possible inhibitor of *E. coli* attachment.
  24. Ofek I, Mirelman D, Sharon N. Adherence of *Escherichia coli* to human mucosal cells mediated by mannose receptors. *Nature*. 1977; 265:623–25. [PubMed: 323718]
  - 25\*. Aronson M, Medalia O, Schori L, et al. Prevention of colonization of the urinary tract of mice with *Escherichia coli* by blocking of bacterial adherence with methyl  $\alpha$ -D-mannopyranoside. *J Infect Dis*. 1979; 139:329–32. First paper describing mannosides as strategy to block type 1 pili in UTI. [PubMed: 376757]
  26. Firon N, Ofek I, Sharon N. Interaction of mannose-containing oligosaccharides with the fimbrial lectin of *Escherichia coli*. *Biochem Biophys Res Commun*. 1982; 105(4):1426–32. [PubMed: 6125146]
  27. Firon N, Ofek I, Sharon N. Carbohydrate specificity of the surface lectins of *Escherichia coli*, *Klebsiella pneumoniae*, and *Salmonella typhimurium*. *Carb Res*. 1983; 120:235–49.
  - 28\*. Firon N, Ashkenazi S, Mirelman D, Ofek I, Sharon N. Aromatic  $\alpha$ -glycosides of mannose are powerful inhibitors of the adherence of type 1 fimbriated *Escherichia coli* to yeast and intestinal epithelial cells. *Infect Immun*. 1987; 55(2):472–76. Discovery of monomeric aryl mannosides as FimH ligands. [PubMed: 3542836]
  29. Andrade JRC. Role of fimbrial adhesiveness in experimental guinea pig kerato conjunctivitis by *Shigella flexneri*. *Rev Microbiol*. 1980; 11(4):117–25.
  30. Neeser J, Koellreutter B, Wuersch P. Oligomannoside-Type Glycopeptides Inhibiting Adhesion of *Escherichia coli* Strains Mediated by Type 1 Pili: Preparation of Potent Inhibitors from Plant Glycoproteins. *Infect Immun*. 1986; 52(4):428–36. [PubMed: 2870987]
  - 31\*. Mydock-McGrane LK, Cusumano ZT, Janetka JW. Mannose-derived FimH antagonists: a promising anti-virulence therapeutic strategy for urinary tract infections and Crohn's disease. *Expert Opin Ther Pat*. 2016; 26(2):175–97. Recent patent literature review on FimH antagonists. [PubMed: 26651364]
  32. Klein T, Abgottsporn D, Wittwer M, et al. FimH antagonists for the oral treatment of urinary tract infections: from design and synthesis to in vitro and in vivo evaluation. *J Med Chem*. 2010; 53(24):8627–41. [PubMed: 21105658]
  33. Rabbani S, Jiang X, Schwardt O, et al. Expression of the carbohydrate recognition domain of FimH and development of a competitive binding assay. *Anal Biochem*. 2010; 407(2):188–95. [PubMed: 20705050]

34. Lindhorst TK, Kotter S, Krallmann-Wenzel U, et al. Trivalent alpha-d-mannoside clusters as inhibitors of type-1 fimbriae-mediated adhesion of Escherichia coli: structural variation and biotinylation. *J Chem Soc Perkin Trans I*. 2001; 8:823–31.
- 35\*. Brument S, Sivignon A, Dumych TI, et al. Thiazolylaminomannosides as potent antiadhesives of type 1 piliated Escherichia coli isolated from Crohn's disease patients. *J Med Chem*. 2013; 56(13):5395–406. Identification of N-mannoside “TazMan” FimH ligands in Crohn's Disease, AIEC bacteria. [PubMed: 23795713]
36. Chalopin T, Dorta DA, Sivignon A, et al. Second generation of thiazolylmannosides, FimH antagonists for E. coli-induced Crohn's disease. *Org Biomol Chem*. 2016; 14(16):3913–25. [PubMed: 27043998]
- 37\*\*. Han Z, Pinkner JS, Ford B, et al. Structure-based drug design and optimization of mannoside bacterial FimH antagonists. *J Med Chem*. 2010; 53(12):4779–92. Discovery of biphenyl and biaryl mannosides, X-ray structure and key SAR. [PubMed: 20507142]
38. Kleeb S, Pang L, Mayer K, et al. FimH antagonists: bioisosteres to improve the in vitro and in vivo PK/PD profile. *J Med Chem*. 2015; 58(5):2221–39. [PubMed: 25666045]
- 39\*\*. Bouckaert J, Berglund J, Schembri M, et al. Receptor binding studies disclose a novel class of high-affinity inhibitors of the Escherichia coli FimH adhesin. *Mol Microbiol*. 2005; 55(2):441–55. X-ray crystal structure of D-Mannose and butylmannoside bound to FimH enabling rational structure-based design of mannosides. [PubMed: 15659162]
40. Pang L, Kleeb S, Lemme K, et al. FimH antagonists: structure-activity and structure-property relationships for biphenyl alpha-D-mannopyranosides. *ChemMedChem*. 2012; 7(8):1404–22. [PubMed: 22644941]
41. Han Z, Pinkner JS, Ford B, et al. Lead optimization studies on FimH antagonists: discovery of potent and orally bioavailable ortho-substituted biphenyl mannosides. *J Med Chem*. 2012; 55(8):3945–59. [PubMed: 22449031]
42. Kranz JK, Schalk-Hihi C. Protein thermal shifts to identify low molecular weight fragments. *Methods Enzymol*. 2011; 493:277–98. [PubMed: 21371595]
43. Niesen F, Berglund H, Vedadi M. The use of differential scanning fluorimetry to detect ligand interactions that promote protein stability. *Nat Protoc*. 2007; 2(2212):2212–21. [PubMed: 17853878]
44. Hultgren S, Schwan W, Schaeffer A, et al. Regulation of production of type 1 pili among urinary tract isolates of Escherichia coli. *Infect Immun*. 1986; 54(3):613–20. [PubMed: 2877947]
- 45\*\*. Mydock-McGrane L, Cusumano Z, Han Z, et al. Antivirulence C-mannosides as antibiotic-sparing, oral therapeutics for urinary tract infections. *J Med Chem*. 2016; 59:9390–408. Report of C-mannoside FimH antagonists with significantly enhance metabolic stability. [PubMed: 27689912]
46. Jarvis C, Han Z, Kalas V, et al. Antivirulence isoquinolone mannosides: optimization of the biaryl aglycone for FimH lectin binding affinity and efficacy in the treatment of chronic UTI. *ChemMedChem*. 2016; 11(4):367–73. [PubMed: 26812660]
47. Abgottspon D, Rölli G, Hosch L, et al. Development of an aggregation assay to screen FimH antagonists. *J Microbiol Methods*. 2010; 82:249–55. [PubMed: 20620174]
48. O'Toole G, Kolter R. Initiation of biofilm formation in *Pseudomonas fluorescens* WCS365 proceeds via multiple, convergent signalling pathways: a genetic analysis. *Mol Microbiol*. 1998; 28(3):449–61. [PubMed: 9632250]
49. Cegelski L, Pinkner J, Hammer N, et al. Small-molecule inhibitors target Escherichia coli amyloid biogenesis and biofilm formation. *Nat Chem Biol*. 2009; 5(12):913–19. [PubMed: 19915538]
50. Pinkner JS, Remaut H, Buelens F, et al. Rationally designed small compounds inhibit pilus biogenesis in uropathogenic bacteria. *Proc Natl Acad Sci USA*. 2006; 103(47):17897–902. [PubMed: 17098869]
51. Blango MG, Mulvey MA. Persistence of uropathogenic Escherichia coli in the face of multiple antibiotics. *Antimicrob Agents Chemother*. 2010; 54(5):1855–63. [PubMed: 20231390]
52. Scharenberg M, Abgottspon D, Cicek E, et al. A flow cytometry-based assay for screening FimH antagonists. *Assay Drug Dev Technol*. 2011; 9(5):455–64. [PubMed: 21675870]

- 53\*. Kalas V, Pinkner JS, Hannan TJ, et al. Evolutionary fine-tuning of conformational ensembles in FimH during host-pathogen interactions. *Sci Adv.* 2017; 3(2):e1601944. Key paper describing FimH conformational variability in UPEC. [PubMed: 28246638]
- 54\*. Eris D, Preston RC, Scharenberg M, et al. The conformational variability of FimH: which conformation represents the therapeutic target? *Chembiochem.* 2016; 17(11):1012–20. Key paper describing differential binding of mannosides to different bacterial strains. [PubMed: 26991759]
55. Sauer MM, Jakob RP, Eras J, et al. Catch-bond mechanism of the bacterial adhesin FimH. *Nat Commun.* 2016; 7:10738. [PubMed: 26948702]
56. Hannan TJ, Mysorekar IU, Hung CS, et al. Early severe inflammatory responses to uropathogenic *E. coli* predispose to chronic and recurrent urinary tract infection. *PLoS Pathog.* 2010; 6(8):e1001042. [PubMed: 20811584]
57. Hannan TJ, Totsika M, Mansfield KJ, et al. Host-pathogen checkpoints and population bottlenecks in persistent and intracellular uropathogenic *Escherichia coli* bladder infection. *FEMS Microbiol Rev.* 2012; 36(3):616–48. [PubMed: 22404313]
58. Hung CS, Dodson KW, Hultgren SJ. A murine model of urinary tract infection. *Nat Protoc.* 2009; 4(8):1230–43. [PubMed: 19644462]
59. Justice SS, Hung C, Theriot JA, et al. Differentiation and developmental pathways of uropathogenic *Escherichia coli* in urinary tract pathogenesis. *Proc Natl Acad Sci USA.* 2004; 101(5):1333–8. [PubMed: 14739341]
60. Schwartz DJ, Conover MS, Hannan TJ, et al. Uropathogenic *Escherichia coli* superinfection enhances the severity of mouse bladder infection. *PLoS Pathog.* 2015; 11(1):e1004599. [PubMed: 25569799]
61. Wright KJ, Seed PC, Hultgren SJ. Development of intracellular bacterial communities of uropathogenic *Escherichia coli* depends on type 1 pili. *Cell Microbiol.* 2007; 9(9):2230–41. [PubMed: 17490405]
- 62\*\*. Cusumano CK, Pinkner JS, Han Z, et al. Treatment and prevention of urinary tract infection with orally active FimH inhibitors. *Sci Transl Med.* 2011; 3(109):109ra15. Demonstration of oral efficacy of a mannoside FimH antagonist in acute and chronic animal models of UTI. First reported *in vivo* efficacy of any anti-virulence therapeutic in a bacterial infection.
- 63\*. Totsika M, Kostakioti M, Hannan TJ, et al. A FimH inhibitor prevents acute bladder infection and treats chronic cystitis caused by multidrug-resistant uropathogenic *Escherichia coli* ST131. *J Infect Dis.* 2013; 208(6):921–28. FimH mannosides are effective at treating EBSL and MDR forms of UPEC. [PubMed: 23737602]
64. Keane WF, Freedman LR. Pyelonephritis in normal mice produced by inoculation of *E. coli* into bladder lumen during water diuresis. *Yale J Biol Med.* 1967; 40(3):231–37. [PubMed: 4870557]
65. Murawski IJ, Maina RW, Malo D, et al. The C3H/HeJ inbred mouse is a model of vesicoureteric reflux with a susceptibility locus on chromosome 12. *Kidney Int.* 2010; 78(3):269–78. [PubMed: 20407478]
66. Nicolas-Chanoine MH, Blanco J, Leflon-Guibout V, et al. Intercontinental emergence of *Escherichia coli* clone O25:H4-ST131 producing CTX-M-15. *J Antimicrob Chemother.* 2008; 61(2):273–81. [PubMed: 18077311]
67. Barnich N, Carvalho FA, Glasser AL, et al. CEACAM6 acts as a receptor for adherent-invasive *E. coli*, supporting ileal mucosa colonization in Crohn disease. *J Clin Invest.* 2007; 117(6):1566–74. [PubMed: 17525800]
68. Carvalho FA, Barnich N, Sivignon A, et al. Crohn's disease adherent-invasive *Escherichia coli* colonize and induce strong gut inflammation in transgenic mice expressing human CEACAM. *J Exp Med.* 2009; 206(10):2179–89. [PubMed: 19737864]
69. Sivignon A, Yan X, Dorta DA, et al. Development of heptylmannoside-based glycoconjugate antiadhesive compounds against adherent-invasive *Escherichia coli* Bacteria associated with Crohn's disease. *mBio.* 2015; 6(6):e01298–15. [PubMed: 26578673]
70. Kuehn MJ, Heuser J, Normark S, et al. P pili in uropathogenic *E. coli* are composite fibers with distinct fibrillar adhesive tips. *Nature.* 1992; 356:252–55. [PubMed: 1348107]
71. Sauer FG, Pinkner JS, Waksman G, et al. Chaperone priming of pilus subunits facilitates a topological transition that drives fiber formation. *Cell.* 2002; 111:543–51. [PubMed: 12437927]



- 72\*. Geibel S, Procko E, Hultgren SJ, et al. Structural and energetic basis of folded protein transport by the FimD usher. *Nature*. 2013; 496:243–46. Paper describing the up to date mechanism of pilus assembly in type 1 pili. [PubMed: 23579681]
73. Remaut H, Rose RJ, Hannan TJ, et al. Donor-strand exchange in chaperone-assisted pilus assembly proceeds through a concerted beta strand displacement mechanism. *Mol Cell*. 2006; 22(6):831–42. [PubMed: 16793551]
74. Sauer FG, Futterer K, Pinkner JS, et al. Structural basis of chaperone function and pilus biogenesis. *Science*. 1999; 285(5430):1058–61. [PubMed: 10446050]
75. Hung CS, Bouckaert J, Hung D, et al. Structural basis of tropism of *Escherichia coli* to the bladder during urinary tract infection. *Mol Microbiol*. 2002; 44(4):903–15. [PubMed: 12010488]
76. Wellens A, Garofalo C, Nguyen H, et al. Intervening with urinary tract Infections using anti-adhesives based on the crystal structure of the FimH oligomannose-3 complex. *PLoS One*. 2008; 3(4):e2040. [PubMed: 18446213]
77. Chen SL, Hung CS, Pinkner JS, et al. Positive selection identifies an in vivo role for FimH during urinary tract infection in addition to mannose binding. *Proc Natl Acad Sci USA*. 2009; 106(52):22439–44. [PubMed: 20018753]
78. Knight SD, Bouckaert J. Structure, function, and assembly of type 1 fimbriae. *Top Curr Chem*. 2009; 288:67–107. [PubMed: 22328027]
79. Bouckaert J, Mackenzie J, de Paz JL, et al. The affinity of the FimH fimbrial adhesin is receptor-driven and quasi-independent of *Escherichia coli* pathotypes. *Mol Microbiol*. 2006; 61(6):1556–68. [PubMed: 16930149]
80. Wellens A, Lahmann M, Touaibia M, et al. The tyrosine gate as a potential entropic lever in the receptor-binding site of the bacterial adhesin FimH. *Biochemistry*. 2012; 51:4790–99. [PubMed: 22657089]
81. Roos G, Wellens A, Touaibia M, et al. Validation of reactivity descriptors to assess the aromatic stacking within the tyrosine gate of FimH. *Med Chem Lett*. 2013; 4:1085–90.
82. Rabbani S, Krammer EM, Roos G, et al. Mutation of Tyr137 of the universal *Escherichia coli* fimbrial adhesin FimH relaxes the tyrosine gate prior to mannose binding. *IUCrJ*. 2017; 4(1):7–23.
83. Sperling O, Fuchs A, Lindhorst TK. Evaluation of the carbohydrate recognition domain of the bacterial adhesin FimH: design, synthesis and binding properties of mannoside ligands. *Org Biomol Chem*. 2006; 4(21):3913–22. [PubMed: 17047870]
- 84\*. Jiang X, Abgottspon D, Kleeb S, et al. Antiadhesion therapy for urinary tract infections—a balanced PK/PD profile proved to be key for success. *J Med Chem*. 2012; 55(10):4700–13. Paper systematically profiling PK and PD of FimH antagonists for UTI. [PubMed: 22519985]
85. Sharon N. Bacterial lectins, cell-cell recognition and infectious disease. *FEBS Lett*. 1987; 217(2):145–57. [PubMed: 2885220]
86. Fiege B, Rabbani S, Preston RC, et al. The tyrosine gate of the bacterial lectin FimH: a conformational analysis by NMR spectroscopy and X-ray crystallography. *Chembiochem*. 2015; 16(8):1235–46. [PubMed: 25940742]
87. Grabosch C, Hartmann M, Schmidt-Lassen J, et al. Squaric acid monoamide mannosides as ligands for the bacterial lectin FimH: covalent inhibition or not? *Chembiochem*. 2011; 12:1066–74. [PubMed: 21472956]
88. Schwardt O, Rabbani S, Hartmann M, et al. Design, synthesis and biological evaluation of mannosyl triazoles as FimH antagonists. *Bioorg Med Chem Lett*. 2011; 19(21):6454–73.
89. Car Z, Hrenar T, Perokovic VP, et al. Mannosylated N-aryl substituted 3-hydroxypyridine-4-ones: synthesis, hemagglutination inhibitory properties, and molecular modeling. *Chem Biol Drug Des*. 2014; 84:393–401. [PubMed: 24674669]
90. Tomasic T, Rabbani S, Gobec M, et al. Branched alpha-D-mannopyranosides: a new class of potent FimH antagonists. *Med Chem Commun*. 2014; 5(8):1247–53.
91. Chandrasekaran V, Kolbe K, Beiroth F, et al. Synthesis and testing of the first azobenzene mannobioside as photoswitchable ligand for the bacterial lectin FimH. *Beilstein J Org Chem*. 2013; 9:223–33. [PubMed: 23399876]
- 92\*. Hartmann M, Papavlassopoulos H, Chandrasekaran V, et al. Inhibition of bacterial adhesion to live human cells: activity and cytotoxicity of synthetic mannosides. *FEBS Lett*. 2012; 586:1459–

65. Paper describing lack of toxicity found for several mannosides against mammalian cells. [PubMed: 22673511]
93. Rodriguez VB, Kidd BA, Interlandi G, et al. Allosteric coupling in the bacterial adhesive protein FimH. *J Biol Chem*. 2013; 288(33):24128–39. [PubMed: 23821547]
94. Yakovenko O, Tchesnokova V, Sokurenko EV, et al. Inactive conformation enhances binding function in physiological conditions. *Proc Natl Acad Sci USA*. 2015; 112(32):9884–9. [PubMed: 26216967]
95. Feenstra T, Thogersen MS, Wieser E, et al. Adhesion of *Escherichia coli* under flow conditions reveals potential novel effects of FimH mutations. *Eur J Clin Microbiol Infect Dis*. 2017; 36(3): 467–78. [PubMed: 27816993]
96. Szunerits S, Zagorodko O, Cogež V, et al. Differentiation of Crohn's disease-associated isolates from other pathogenic *Escherichia coli* by fimbrial adhesion under shear force. *Biology (Basel)*. 2016; 5(2):14.
97. Mockl L, Fessele C, Despras G, et al. En route from artificial to natural: evaluation of inhibitors of mannose-specific adhesion of *E. coli* under flow. *Biochim Biophys Acta*. 2016; 1860(9):2031–6. [PubMed: 27345501]
98. Di L, Kerns EH. Profiling drug-like properties in discovery research. *Curr Opin Chem Biol*. 2003; 7(3):402–08. [PubMed: 12826129]
99. Ito S, Ando H, Ose A, et al. Relationship between the urinary excretion mechanisms of drugs and their physicochemical properties. *J Pharm Sci*. 2013; 102(9):3294–301. [PubMed: 23712676]
- 100\*. de Ruyck J, Lensink MF, Bouckaert J. Structures of C-mannosylated anti-adhesives bound to the type 1 fimbrial FimH adhesin. *IUCrJ*. 2016; 3(Pt 3):163–7. First reported X-ray structural information on simple C-linked biphenyl mannosides.
101. Bennani YL, Cadilhac C, Das SK, et al. Mannose derivatives for treating bacterial infections. WO/2013/134415. 2013
102. Bennani YL, Liu B. Mannose derivatives for treating bacterial infections. WO/2014/055474. 2014
- 103\*. Dietrich, E., Poisson, C., Gallant, M., et al. Mannoside derivatives for treating bacterial infections. WO2014/165107A2. 2014. Vertex patent covering mannose dimers which could include clinical candidate EB8018
- 104\*. Schönemann W, Kleeb S, Dätwyler P, et al. Prodruggability of carbohydrates — oral FimH antagonists. *Can J Chem*. 2016:1–11. Prodrug approach to mannosides.
- 105\*. Kleeb S, Jiang X, Frei P, et al. FimH antagonists: phosphate prodrugs improve oral bioavailability. *J Med Chem*. 2016; 59(7):3163–82. Phosphate prodrug approach to mannosides. [PubMed: 26959338]
106. Lee RT, Lee YC. Affinity enhancement by multivalent lectin-carbohydrate interaction. *Glycoconj J*. 2000; 17:543–51. [PubMed: 11421347]
107. Nagahori N, Lee RT, Nishimura SI, et al. Inhibition of adhesion of type 1 fimbriated *Escherichia coli* to highly mannosylated ligands. *Chembiochem*. 2002; 3:836–44. [PubMed: 12210984]
108. Papadopoulos A, Shiao TC, Roy R. Diazo transfer and click chemistry in the solid phase syntheses of lysine-based glycodendrimers as antagonists against *Escherichia coli* FimH. *Mol Pharm*. 2012; 9:394–403. [PubMed: 22201286]
109. Chalopin T, Brissonnet Y, Sivignon A, et al. Inhibition profiles of mono- and polyvalent FimH antagonists against 10 different *Escherichia coli* strains. *Org Biomol Chem*. 2015; 13:11369–75. [PubMed: 26440382]
110. Yan X, Sivignon A, Yamakawa N, et al. Glycopolymers as antiadhesives of *E. coli* strains inducing inflammatory bowel diseases. *Biomacromolecules*. 2015; 16:1827–36. [PubMed: 25961760]
111. Bouckaert J, Li Z, Xavier C, et al. Heptyl alpha-D-mannosides grafted on a beta-cyclodextrin core to interfere with *Escherichia coli* adhesion: an in vivo multivalent effect. *Chemistry*. 2013; 19(24):7847–55. [PubMed: 23595913]
112. Gouin SG, Wellens A, Bouckaert J, et al. Synthetic multimeric heptyl mannosides as potent antiadhesives of uropathogenic *Escherichia coli*. *ChemMedChem*. 2009; 4(5):749–55. [PubMed: 19343765]

113. Yan X, Sivignon A, Barnich N, et al. A library of heptyl mannose-functionalized copolymers with distinct compositions, microstructures and neighboring non-sugar motifs as potent antiadhesives of type 1 pilated *E. coli*. *Polym Chem*. 2016; 7:2674–83.
114. Almant M, Moreau V, Kovensky J, et al. Clustering of *Escherichia coli* type-1 fimbrial adhesins by using multimeric heptyl  $\alpha$ -D-mannoside probes with a carbohydrate core. *Chem Eur J*. 2011; 17:10029–38. [PubMed: 21774001]
115. Lindhorst TK, Kieburg C, Krallmann-Wenzel U. Inhibition of the type 1 fimbriae-mediated adhesion of *Escherichia coli* to erythrocytes by multiantennary  $\alpha$ -mannosyl clusters: the effect of multivalency. *Glycoconj J*. 1998; 15(6):605–13. [PubMed: 9881767]
116. Kötter S, Krallmann-Wenzel U, Ehlers S, et al. Multivalent ligands for the mannose-specific lectin on type 1 fimbriae of *Escherichia coli*: syntheses and testing of trivalent  $\alpha$ -D-mannoside clusters. *J Chem Soc Perkin Trans I*. 1998:2193–200.
117. Schierholt A, Hartmann M, Lindhorst TK. Bi- and trivalent glycopeptide mannopyranosides as inhibitors of type 1 fimbriae-mediated bacterial adhesion: variation of valency, aglycon and scaffolding. *Carb Res*. 2011; 346:1519–26.
118. Barras A, Martin FA, Bande O, et al. Glycan-functionalized diamond nanoparticles as potent *E. coli* anti-adhesives. *Nanoscale*. 2013; 5:2307–16. [PubMed: 23396565]
119. Durka M, Buffet K, Iehl J, et al. The functional valency of dodecamannosylated fullerenes with *Escherichia coli* FimH—towards novel bacterial antiadhesives. *Chem Commun*. 2011; 47:1321–23.
120. Touaibia M, Wellens A, Shiao TC, et al. Mannosylated G(0) dendrimers with nanomolar affinities to *Escherichia coli* FimH. *ChemMedChem*. 2007; 2(8):1190–201. [PubMed: 17589887]
- 121\*. Sattin S, Bernardi A. Glycoconjugates and glycomimetics as microbial anti-adhesives. *Trends Biotechnol*. 2016; 34(6):483–95. Nice review of multivalent ligands of FimH and other bacterial lectins. [PubMed: 26875976]
- 122\*. Cecioni S, Imbert A, Vidal S. Glycomimetics versus multivalent glycoconjugates for the design of high affinity lectin ligands. *Chem Rev*. 2015; 115(1):525–61. Excellent review on the glycodendrimer inhibitors of lectins in drug discovery. [PubMed: 25495138]
- 123\*. Ramtohl YK., Das, SK., Cadilhac, C., et al. Mannose derivatives for treating bacterial infections. WO/2014/100158. 2014. Vertex patent which might cover clinical candidate EB8018

### Highlights

- Anti-adhesive compounds called mannosides, which bind and inhibit the virulence factor FimH of uropathogenic *E. coli* (UPEC) and adherent invasive *E. coli* (AIEC) bacteria, have become a widely pursued alternative therapeutic strategy to antibiotics in urinary tract infection (UTI) and Crohn's Disease (CD).
- Several diverse biochemical binding, biophysical and cell-based functional assays have been employed to measure FimH mannoside antagonist potency *in vitro*.
- Multiple *in vivo* mouse models have been developed to evaluate the efficacy of mannosides in acute and chronic UTI treatment and prevention as well as in CD.
- Understanding the structural biology of the FimH lectin domain and the key interactions of residues which participate in tight binding mainly to the aglycone portion of mannosides is critical to the design of potent FimH antagonists.
- X-ray structure-guided ligand design has been extensively utilized in the discovery and optimization of small molecule aryl mannoside FimH antagonists.
- Varied structural modifications to both the aryl aglycone and sugar portion of aryl mannosides have been employed in lead optimization of FimH mannosides resulting in the discovery of extremely potent series of biaryl mannosides.
- Medicinal chemistry directed adjustments have resulted in the development of *O*-mannoside prodrugs and new *C*-mannosides with significantly improved efficacy and drug-like properties, including increased oral bioavailability and metabolic stability.
- Multimeric derivatives of mannosides with limited or no oral bioavailability have been pursued as drugs targeting AIEC in the gut. As a result, clinical candidate EB8018 was developed and entered Phase 1 trials in January of 2017 in CD patients.

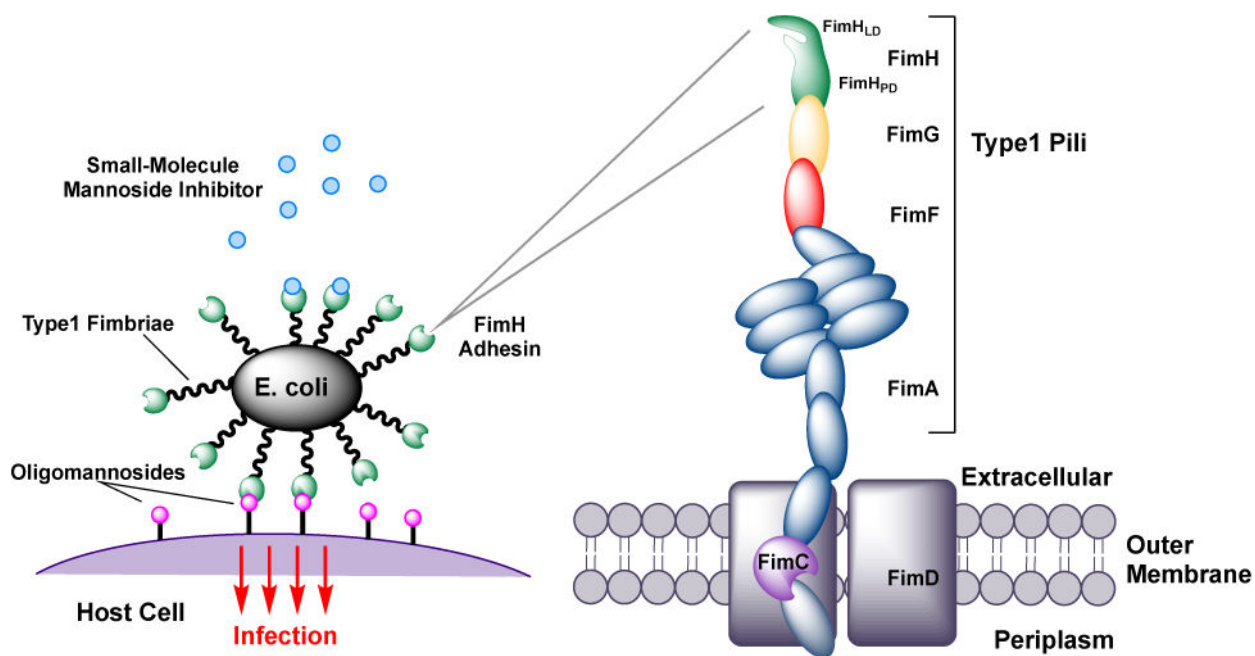
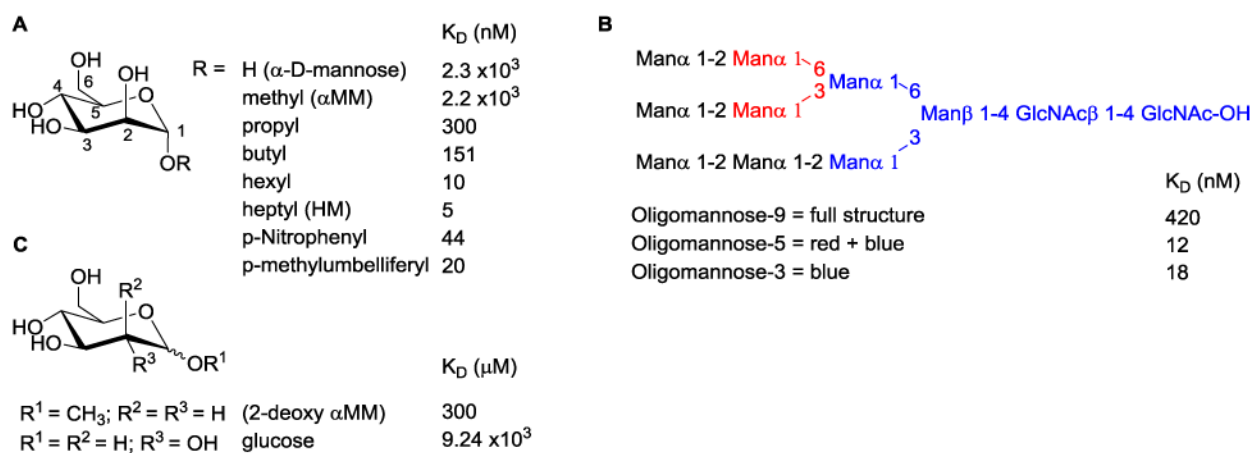


**Figure 1.** Molecular recognition of mannosylated receptors on the bladder surface by FimH adhesin of UPEC, residing on the outer tips of type 1 pili. Therapeutic rationale for FimH mannoside ligands in UTI and CD is to block adherence and invasion of bacteria.



$K_D$  determined by SPR affinity measurements, <sup>a</sup>[bouckaert 2005], <sup>b</sup>[Bouckaert 2006]

**Figure 2.**  
FimH ligand binding affinity of **A.** early synthetic mannosides **B.** oligomannose-9 and subunits and **C.** other sugars.



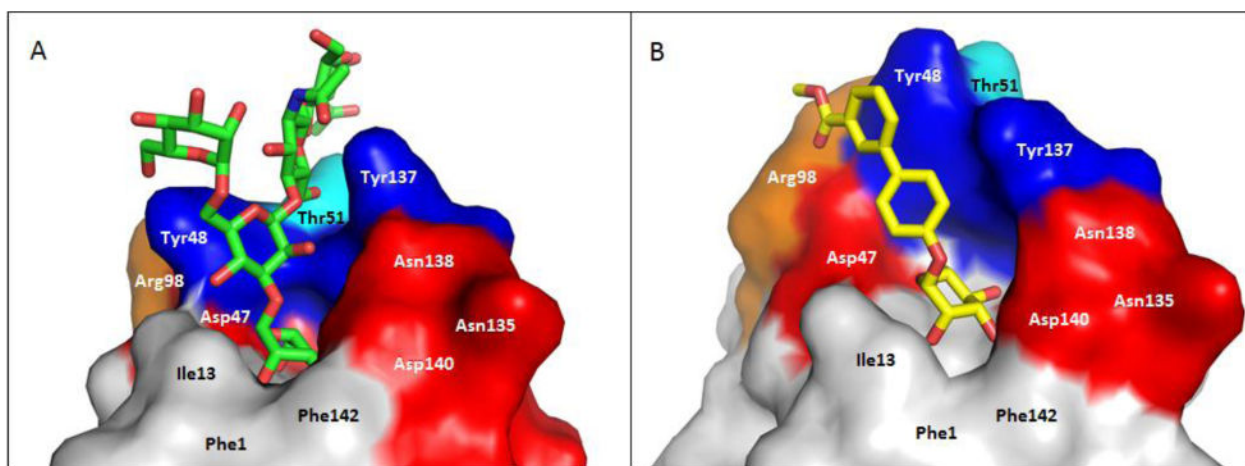


**Figure 3.**

Co-crystal structures of FimH and **A.** oligomannose-3, bound within an open tyrosine gate in an 'in-docking' mode (PDB code: **2VCO**) and **B.** compound **6**, bound in a closed tyrosine gate in an 'outdocking' mode (PDB code: **3MCY**). The surface of the FimH receptor-binding site is subdivided into its hydrophobic support platform (grey; Phe142, Phe1 and Ile13), its polar pocket (red; Asn135, Asn138 and Asp140, and not shown Asn46, Asp47, Asp54, Gln133), the tyrosine gate (blue; Tyr137, Tyr48, and not shown Ile52) and Thr51 (cyan).

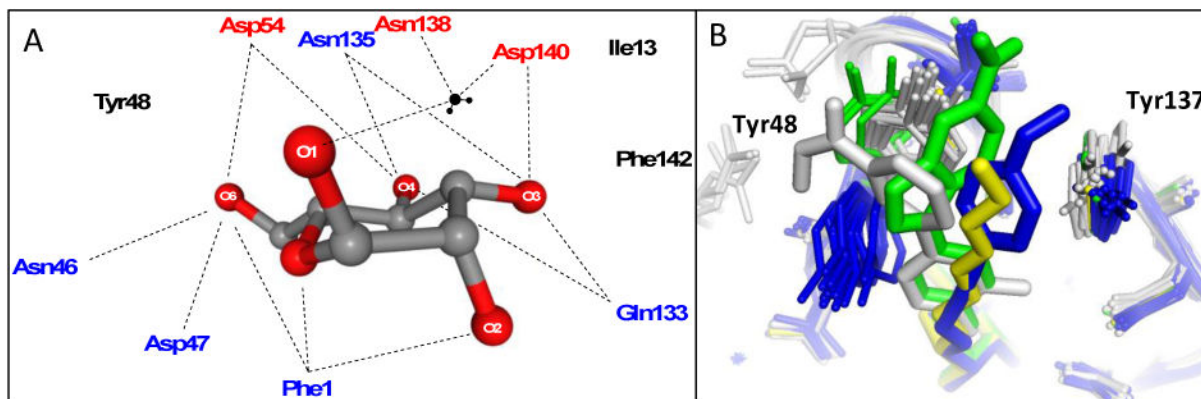


**Figure 4.**

**A.** Schematic of residues in the polar mannose-binding pocket of the FimH lectin domain highlighting the extensive network of electrostatic and H-bonding interactions of  $\alpha$ -D-mannose with FimH. These interactions are responsible for the exquisite stereochemical specificity of FimH-containing bacteria for mannose. **B.** Binding pocket overlay of all reported FimH-mannoside X-ray structures showing the varied conformations of the tyrosine gate, with Tyr48 in grey (closed), blue (open) and green (open twisted), and the Tyr137 position invariant. Representative ligands shown are heptyl mannoside (yellow; **4LOV**), 29 (green; **4X5Q**), 18b (blue; **4AV0**), and 25 (grey; **5F3F**).

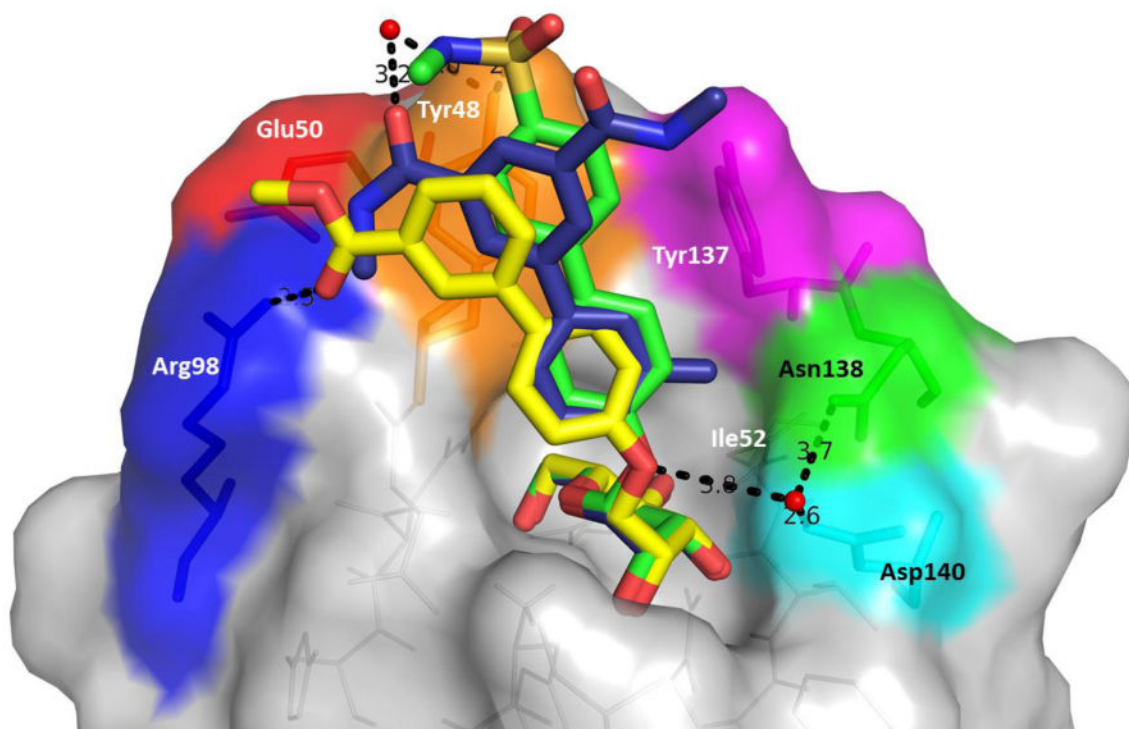


**Figure 5.** Overlay of 6 (yellow; **3MCY**), 16 (green; **4CSS**), 15 (blue; **5F2F**) bound to the FimH lectin domain. Proximal *ortho*-pocket defined by residues Ile52, Asn138, Tyr137; Salt bridge defined by residues Arg98, Glu50; tyrosine gate defined by residues Tyr48, Tyr137, Thr51 (not shown). H-bonds to salt bridge and Tyr48 and Asp140 indicated with distances.

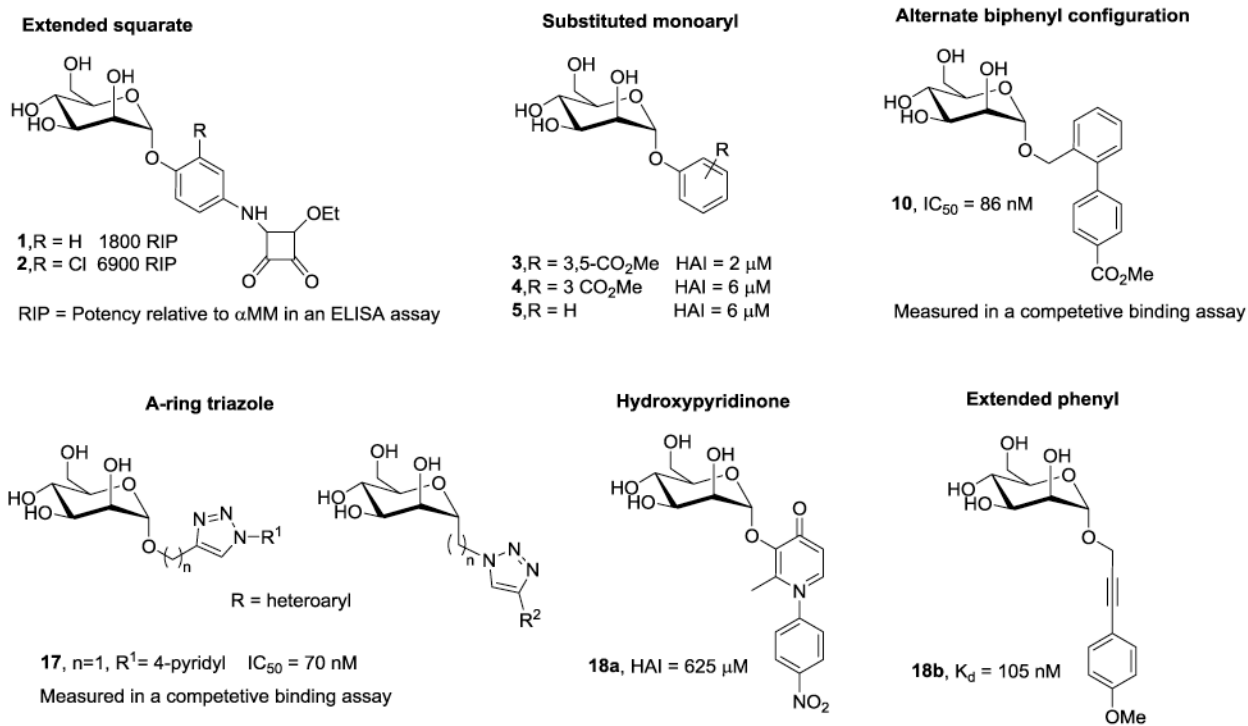


**Figure 6.**  
Structural diversity and activity of FimH mannoside antagonists.

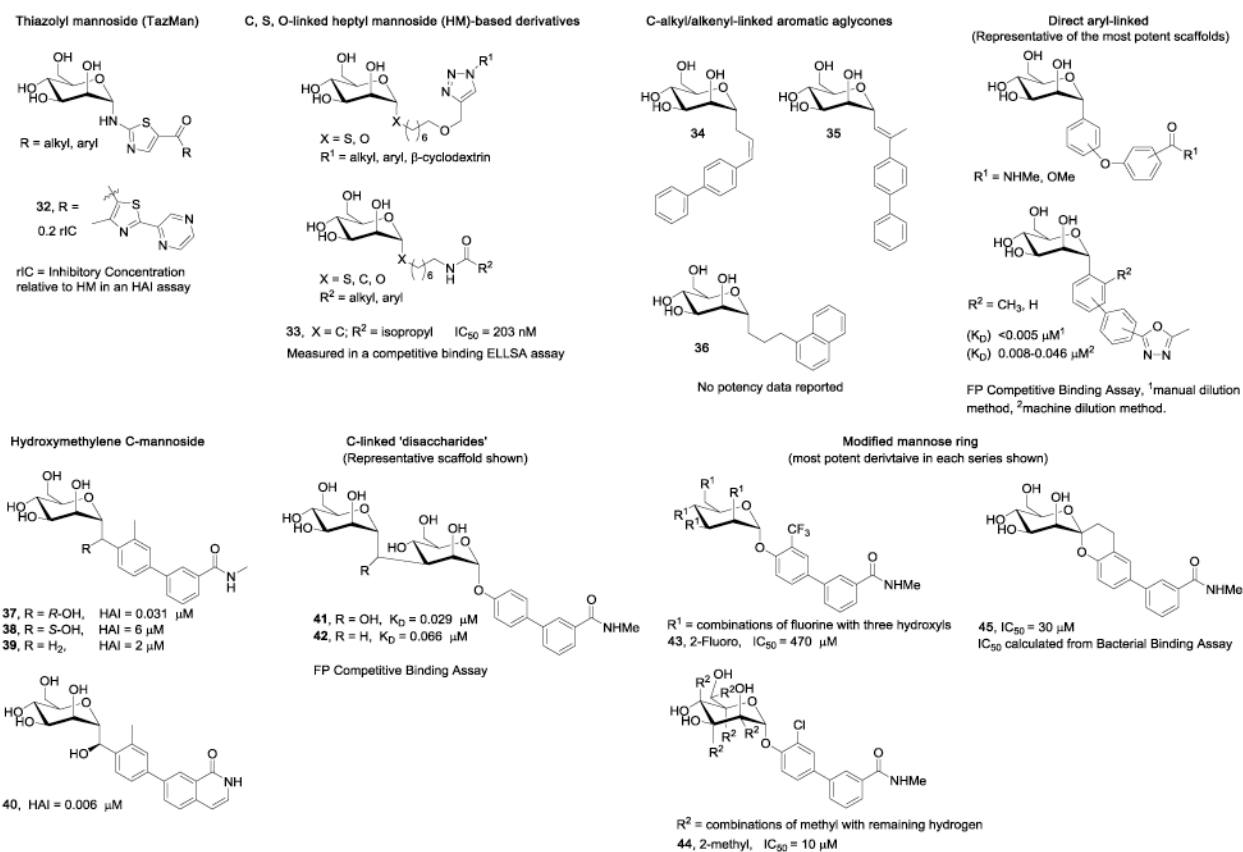


**Figure 7.**  
Examples of medicinal chemistry modifications to the mannoside glycosidic bond.

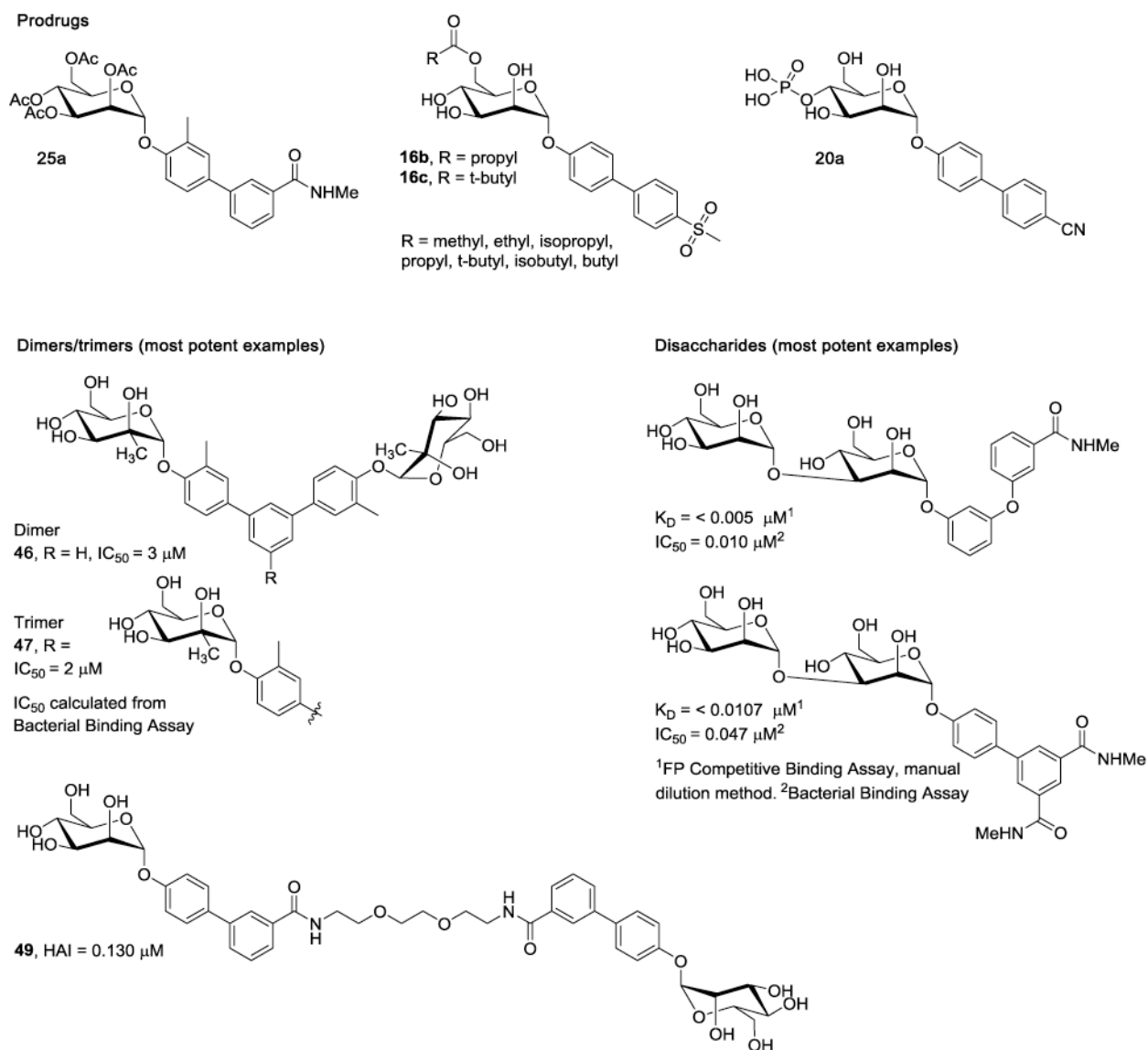


**Figure 8.**  
Structures of mannoside prodrugs, multivalent, and disaccharide antagonists.

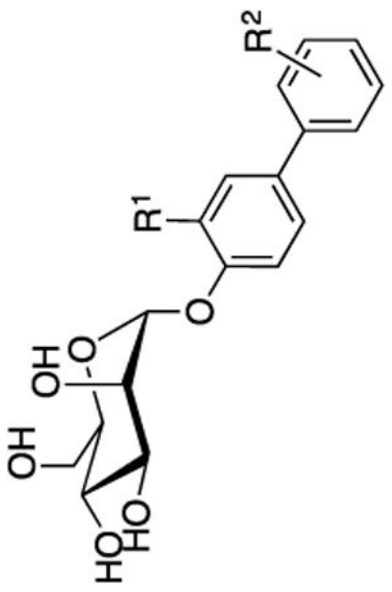


**Table 1**  
**Correlation of assay results in determining FimH binding and biological activity**

Assay	$\alpha$ -D-mannose	$\alpha$ -methyl mannoside ( $\alpha$ .MM)	$\alpha$ -heptyl mannoside (HM)
Disaggregation IC <sub>50</sub>	--	BLQ <sup>a</sup>	~78 $\mu$ M
HAI – EC <sub>90</sub>	>1 mM	>1 mM	15 $\mu$ M
Aggregometry IC <sub>50</sub>	--	--	77 $\mu$ M
Biofilm IC <sub>50</sub>	--	--	20 $\mu$ M
DSF T <sub>m</sub> (°C)	--	~64.5	69.8
FP-EC <sub>50</sub>	--	--	89 $\mu$ M
Cell-free Binding IC <sub>50</sub>	--	--	73 nM
Radiolabel K <sub>D</sub>	4.1 $\times$ 10 <sup>3</sup> nM	2.4 $\times$ 10 <sup>3</sup> nM	32 nM
SPR K <sub>D</sub>	2.3 $\times$ 10 <sup>3</sup> nM	2.2 $\times$ 10 <sup>3</sup> nM	5 nM
BLI K <sub>D</sub>	--	61 nM	--
ELLSA IC <sub>50</sub>	--	--	0.16 $\mu$ M

<sup>a</sup>BLQ, below level of quantification

**Table 2**  
**Structures and SAR of biphenyl mannosides with H-bonding acceptors**



Cmpd	R <sup>1</sup>	R <sup>2</sup>	Binding IC <sub>50</sub> [nM]	FP K <sub>D</sub> [nM]	Agg IC <sub>50</sub> [μM]	HAIEC <sub>50</sub> [nM]	Biofilm IC <sub>50</sub> [nM]	DSF Temp [°C]
6	H	3-CO <sub>2</sub> Me	--	--	--	1000	940	73.39
7	H	3,5-CO <sub>2</sub> Me	--	--	--	150	--	72.53
8	H	4-CO <sub>2</sub> Me	10.4	--	42	4000	--	68.69
9	H	4-CO <sub>2</sub> H	17.1	--	45	--	--	--
11	F	3-CO <sub>2</sub> Me	--	--	--	750	--	--
12	Cl	3-CO <sub>2</sub> Me	--	--	--	30	260	--
13	Cl	4-CO <sub>2</sub> Me	4.8	--	9	--	--	--
14	Cl	4-CO <sub>2</sub> H	6.7	--	10	--	--	--
15	CH <sub>3</sub>	3,5-CONHMe	--	--	--	16	73	75.76
16	H	4-SO <sub>2</sub> NHMe	--	2.7	--	--	--	--
16a	H	4-SO <sub>2</sub> Me	--	1.7	--	--	--	--
19	H	3,5-CONHMe	--	--	--	375	740	72.53
20	Cl	4-CN	--	<1	--	--	--	--
25	CH <sub>3</sub>	3-CONHMe	--	--	--	60	160	74.46
31	H	4-C(O)-morpholine	--	3.0	--	--	--	--

Author Manuscript

Author Manuscript

Author Manuscript

Author Manuscript

Cmpd	R <sup>1</sup>	R <sup>2</sup>	Binding IC <sub>50</sub> [nM]	FP K <sub>D</sub> [nM]	Agg IC <sub>50</sub> [μM]	HAI EC <sub>50</sub> 0 [nM]	Biofilm IC <sub>50</sub> [nM]	DSF Temp [°C]
48	H	3-CONHMe	---	---	--	500	1350	73.38

Author Manuscript

Author Manuscript

Author Manuscript

Author Manuscript

**Table 3**  
***In vitro* physical property and PK data of selected FimH antagonists**

Cmpd	Log D <sub>7.4</sub>	Solubility [µg/mL]/pH	PAMPA Log P <sub>e</sub> [log 10 <sup>-6</sup> cm/s]	Caco-2 P <sub>app</sub> [10 <sup>-6</sup> cm/s]			Metabolic Stability t <sub>1/2</sub> [min]
				A→B	B→A	PPB [%]	
<b>8</b>	2.1	33.8/6.5	-4.7	--	--	93	--
<b>9</b>	-0.8	>3000/6.6	ND	--	--	73	>60
<b>13</b>	2.3	11.9/6.5	-4.6	--	--	94	--
<b>14</b>	-0.8	>3000/6.5	ND	--	--	89	--
<b>16</b>	0.7	>250/7.4	-8.6	0.28	1.82	>99	>60
<b>16a</b>	0.4	246	-7.2	0.4	1.8	--	--
<b>16b</b>	1.8	145	-4.7	17.3	23.5	--	--
<b>16c</b>	2.3	58	-4.6	14.1	19.8	--	--
<b>17</b>	0.24	ND	-8.7	--	--	--	>3000
<b>20</b>	2.1	192/7.4	-5.2	2.2	22.1	89	>60
<b>28</b>	1.8	31.5/6.5	-4.7	--	--	98	--
<b>29</b>	1.9	24/6.5	-5.5	2.9	39.3	95	--
<b>30</b>	1.9	3.6/6.5	-5.7	--	--	99	--
<b>31</b>	0.2	>250/7.4	-7.8	0.18	1.30	48	>60

**Table 4**  
**SAR of optimized mannosides containing fused heteroaryl B-rings**

Cmpd	R <sup>1</sup>	R <sup>2</sup>	R <sup>3</sup>	HAI EC <sub>50</sub> [nM]	Biofilm IC <sub>50</sub> [nM]	DSF Temp [°C]
21	H	H	--	100	--	--
22	--	--	H	250	--	--
23	CH <sub>3</sub>	H	--	31	130	75.5
24	--	--	CH <sub>3</sub>	62	140	75.0
26	CH <sub>3</sub>	CH <sub>2</sub> C(O)NH(3-pyridyl)	--	1	18	--
27	CH <sub>3</sub>	C(O)NH(3-pyridyl)	--	62	--	--

	R <sup>1</sup>	R <sup>2</sup>	X-X	Binding IC <sub>50</sub> [nM]	Aggregation IC <sub>50</sub> [μM]
28	Cl	H	CH=CH	14.9	8.3
29	H	NO <sub>2</sub>	CH <sub>2</sub> -CH <sub>2</sub>	20	26.9
30	Cl	NO <sub>2</sub>	CH <sub>2</sub> -CH <sub>2</sub>	2.4	3.4

**Table 5**  
**In vivo PK data for selected lead mannosides in the mouse and rat**

Cmpd	Mouse plasma					Mouse urine			
	Dose/admin [mg/kg]	CL <sub>tot</sub> [mL/h]	V <sub>t</sub> [mL]	AUC [ $\mu\text{g}^* \text{h/mL}$ ]	t <sub>1/2</sub> [h]	AUC [ $\mu\text{g}^* \text{h/mL}$ ]	T>MIC [h]	C <sub>max</sub> [ $\mu\text{g/mL}$ ]	
HM	50/iv	--	--	34.3	--	2469	--	951.4	
9	50/iv	53.1	25.2	23.5	0.33	140*	--	300	
14	50/iv	--	--	20.8	--	210	4	588.4	
28	25/iv	--	--	8.2	--	19.3	0	--	
29	1/iv	--	--	2.2	--	586	>8	--	
30	0.05/iv	--	--	3.5	--	33.4	8	--	
16	50/iv	7.1	19.5	175.1	1.9	--	--	387	
31	50/iv	49.4	28.3	25.3	0.4	--	--	4611	
20	0.625/iv	218	52.8	0.07	0.17	--	--	10	
	7.7/po	--	--	--	--	107	--	23.6	
20a	10/po	--	--	--	--	226	--	57.0	
Cmpd	Rat plasma					Rat urine			
	Dose/admin [mg/kg]	Cl <sub>obs</sub> [mL/min <sup>*</sup> kg]	V <sub>dis</sub> [L/kg]	t <sub>1/2</sub> [h]	[F%]	AUC [ $\text{ng}^* \text{h/mL}$ ]	C <sub>avg</sub> [ng/mL] (0-8h)	C <sub>avg</sub> [ng/mL] (8-24h)	
19	3/iv	24.7	0.91	0.42	--	1517	--	--	
25	3/iv	98.4	1.3	0.31	--	521	--	--	
	10/po	--	--	2.85	1.34	23.2	2360	212	
23	3/iv	408	6.7	0.28	--	126	--	--	
	10/po	--	--	<3	7.05	29.6	802	65.7	
37	3/iv	34.9	0.74	0.49	--	1440	--	--	
	10/po	--	--	3.53	1.95	93.7	1619	193	

\* determined in a different study